

AN INVESTIGATION OF THE BATCH  
BUBBLING PROCESS

A THESIS

Presented to

The Faculty of the Division of Graduate  
Studies and Research

By

Steven Wayne Couch

In Partial Fulfillment


of the Requirements for the Degree  
Master of Science in Mechanical Engineering


Georgia Institute of Technology

March, 1973


AN INVESTIGATION OF THE BATCH  
BUBBLING PROCESS

Approved:

  
\_\_\_\_\_  
N. Zuber, Chairman

  
\_\_\_\_\_  
W. Wulff

  
\_\_\_\_\_  
C. W. Gorton

  
\_\_\_\_\_  
C. S. Martin

Date approved by Chairman: March 2, 1973

## ACKNOWLEDGMENTS

I would like to thank my advisor, Dr. Novak Zuber, for introducing me to this subject and for his guidance and assistance throughout this investigation.

I wish to extend my appreciation to Drs. C. S. Martin, C. W. Gorton, and W. Wulff for their review of this thesis and their helpful suggestions.

The staff of the School of Mechanical Engineering is to be commended for their assistance in the design and construction of the apparatus.

## TABLE OF CONTENTS

	Page
ACKNOWLEDGMENTS. . . . .	ii
LIST OF TABLES . . . . .	iv
LIST OF ILLUSTRATIONS. . . . .	v
NOMENCLATURE . . . . .	viii
SUMMARY. . . . .	x
Chapter	
I. INTRODUCTION. . . . .	1
1.1 Significance of the Problem	
1.2 Review of Literature	
1.3 Purpose	
II. EXPERIMENTATION . . . . .	16
2.1 Apparatus	
2.2 Instrumentation	
2.3 Experimental Procedure	
III. RESULTS AND DISCUSSION. . . . .	27
IV. CONCLUSIONS AND RECOMMENDATIONS . . . . .	61
APPENDIX A . . . . .	65
APPENDIX B . . . . .	70
APPENDIX C . . . . .	73
REFERENCES . . . . .	79



## LIST OF TABLES

Table		Page
1.	Drag Coefficients and Terminal Velocities (for the regions given on Figure 27) . . . . .	68
2.	Terminal Velocity of Single Gas Bubbles in Liquids . . . . .	69
3.	Data for 11.5 Inch I.D. Test Section Using the 70 $\mu$ Porous Plate. . . . .	74
4.	Data for 11.5 Inch I.D. Test Section Using the 70 $\mu$ Porous Plate. . . . .	75
5.	Data for 11.5 Inch I.D. Test Section Using the 120 $\mu$ Porous Plate . . . . .	76
6.	Data for 11.5 Inch I.D. Test Section Using the 120 $\mu$ Porous Plate . . . . .	77
7.	Data for 4.0 Inch I.D. Test Section Using the 70 $\mu$ Porous Plate. . . . .	78

## LIST OF ILLUSTRATIONS

Figure		Page
1.	A Sample of the Graphs to be Used in the Analysis of the Data. . . . .	8
2.	Overall View of Experimental Apparatus. . . . .	17
3.	Cross Section of Air Chamber and Bottom Flange Assembly for the 11.5 Inch I.D. Test Section. . . . .	18
4.	Cross Section of Air Chamber and Lower Assembly for the 4.0 Inch I.D. Test Section . .	20
5.	Volumetric Flux Density Versus Void Fraction for the 11.5 Inch I.D. Test Section Using the 120 $\mu$ Porous Plate . . . . .	28
6.	Volumetric Flux Density Versus Void Fraction for the 11.5 Inch I.D. Test Section Using the 70 $\mu$ Porous Plate. . . . .	29
7.	Volumetric Flux Density Versus Void Fraction for the 4.0 Inch I.D. Test Section. . . . .	30
8.	Volumetric Flux Density Versus Void Fraction for the 11.5 Inch I.D. Test Section Using the 70 $\mu$ Porous Plate. . . . .	33
9.	Volumetric Flux Density Versus Void Fraction for the 11.5 Inch I.D. Test Section Using the 120 $\mu$ Porous Plate . . . . .	34
10.	Volumetric Flux Density Versus Void Fraction for the 11.5 Inch I.D. Test Section Using the 70 $\mu$ Porous Plate. . . . .	36
11.	Volumetric Flux Density Versus Void Fraction for the 11.5 Inch I.D. Test Section Using the 120 $\mu$ Porous Plate . . . . .	37
12.	Volumetric Flux Density Versus Void Fraction for the 11.5 Inch I.D. Test Section Using the 70 $\mu$ Porous Plate. . . . .	38

Figure		Page
13.	Volumetric Flux Density Versus Void Fraction for the 11.5 Inch I.D. Test Section Using the 120 $\mu$ Porous Plate. . . . .	39
14.	Volumetric Flux Density Versus Void Fraction for the 11.5 Inch I.D. Test Section Using the 70 $\mu$ Porous Plate . . . . .	40
15.	Volumetric Flux Density Versus Void Fraction for the 11.5 Inch I.D. Test Section Using the 120 $\mu$ Porous Plate. . . . .	41
16.	Velocity of the Gas Phase Versus Volumetric Flux Density for the 11.5 Inch I.D. Test Section Using the 70 $\mu$ Porous Plate . . . . .	44
17.	Velocity of the Gas Phase Versus Volumetric Flux Density for the 11.5 Inch I.D. Test Section Using the 120 $\mu$ Porous Plate. . . . .	45
18.	Velocity of the Gas Phase Versus Volumetric Flux Density for the 11.5 Inch I.D. Test Section Using the 70 $\mu$ Porous Plate . . . . .	47
19.	Velocity of the Gas Phase Versus Volumetric Flux Density for the 11.5 Inch I.D. Test Section Using the 70 $\mu$ Porous Plate . . . . .	48
20.	Velocity of the Gas Phase Versus Volumetric Flux Density for the 11.5 Inch I.D. Test Section Using the 120 $\mu$ Porous Plate . . . . .	49
21.	Velocity of the Gas Phase Versus Volumetric Flux Density for the 11.5 Inch I.D. Test Section Using the 70 $\mu$ Porous Plate . . . . .	50
22.	Velocity of the Gas Phase Versus Volumetric Flux Density for the 11.5 Inch I.D. Test Section Using the 70 $\mu$ Porous Plate . . . . .	53
23.	Velocity of the Gas Phase Versus Volumetric Flux Density for the 11.5 Inch I.D. Test Section Using the 70 $\mu$ Porous Plate . . . . .	54
24.	Velocity of the Gas Phase Versus Volumetric Flux Density for the 11.5 Inch I.D. Test Section Using the 120 $\mu$ Porous Plate. . . . .	55

Figure		Page
25.	Velocity of the Gas Phase Versus Volumetric Flux Density for the 11.5 Inch I.D. Test Section Using the 70 $\mu$ Porous Plate. . . . .	56
26.	Velocity of the Gas Phase Versus Volumetric Flux Density for the 4.0 Inch I.D. Test Section Using the 70 $\mu$ Porous Plate. . . . .	58
27.	Terminal Velocity of Rise of Air Bubbles as a Function of Bubble Size . . . . .	67
28.	Control Volume for the Determination of the Volumetric Flux Density from Measurable Quantities. . . . .	71

## NOMENCLATURE

$A$	cross sectional area of the test section
$A_c$	cross sectional area of the core region of the flow
$A_p$	pressure independent parameter for a given apparatus
$A_{pl}$	cross sectional area of the porous plate
$C_D$	drag coefficient (dimensionless)
$C_o$	distribution parameter
$d$	diameter of bubble
$D$	diameter of the test section (or tube)
$g$	acceleration due to gravity
$h_1$	initial manometer reading
$\Delta h$	change in manometer reading
$j_1$	volumetric flux density of liquid phase
$j_2$	volumetric flux density of gas phase
$j_m$	volumetric flux density of mixture
$L/D$	ratio of height of water column to its diameter
$P_o$	exit pressure of flowmeter
$P_p$	pressure at surface of porous plate
$Q$	flowmeter reading
$Q_o$	corrected flowmeter reading
$Q_2$	volumetric flow rate of air entering test section
$r_e$	equivalent bubble radius
$Re_b$	Reynolds number based on bubble size and velocity

$S$	correction factor for flowmeter
$T_o$	temperature of air flowing through flowmeter
$T_p$	temperature of air at surface of porous plate
$u_r$	relative velocity between the phases
$u_t$	terminal velocity of rise of a bubble
$V_b$	bubble volume
$v_2$	$= j_2/\alpha$ velocity of gas phase
$v_{2j}$	drift velocity of gas phase
$\alpha$	void fraction, holdup, or volumetric concentration
$\phi$	ratio of the volume of the liquid entrained by a bubble to the volume of the bubble
$\rho_1$	density of liquid phase
$\rho_2$	density of gas phase
$\sigma$	surface tension
$\langle \rangle$	average value of

## SUMMARY

The process of bubbling air through water in a batch system is investigated in order to attain a more thorough understanding of the characteristics and limits of the distinct flow regimes that can occur. The effect of plate porosity and  $L/D$  on the flow system is analyzed.

Experiments are performed on an apparatus designed and constructed specifically for this investigation. The basic apparatus consists of two vertical tubes with inside diameters of 11.5 and 4.0 inches. The air is introduced into the system through porous plates located at the bottom of each tube. The data is analyzed to determine the void fraction as a function of the plate porosity,  $L/D$ , and gas flow rate.

Four distinct two-phase flow regimes and a transition region are experimentally observed and analyzed. These regimes are the laminar, churn-turbulent, slug flow, and pseudo-jet flow.

The void fraction for the laminar regime is independent of plate porosity and  $L/D$  but is linearly dependent on the gas flow rate (or volumetric flux density). For the churn-turbulent, slug flow, and pseudo-jet flow regimes, the void fraction is independent of plate porosity but increases for increasing  $L/D$  at constant gas flow rates.

For the 11.5 inch inside diameter test section, the

churn-turbulent regime is found to exist for  $L/D$  less than 5. For  $L/D$  of 5 or greater, the system develops into the slug flow regime.

On a graph of the velocity of the air phase versus the volumetric flux density, the churn-turbulent and slug flow regimes can be represented by single straight lines, whereas the pseudo-jet flow regime is characterized by parallel straight lines of constant  $L/D$ .

The experimental results are in qualitative agreement with the present theories. However, these theories cannot be used to predict the experimental results because insufficient information is available for the determination of the distribution parameter.

Recommendations are offered for continued experimentation and analysis pertaining to the batch bubbling process.



## CHAPTER I

### INTRODUCTION

#### 1.1 Significance of the Problem

The flow of two-phase mixtures and, in particular, dispersed flow in a batch process such as that arising from the bubbling of gases through stagnant\* liquids has much relevance to some of today's modern industrial processes. The petroleum industry, for instance, is constantly confronted with the problems associated with the extraction of two or even three-phase mixtures involving gas, oil, and water from the earth. In the chemical process industry, in steam generation equipment, in nuclear reactor design, or in any other facet of industry that deals with heat transfer, two-phase flows can arise from the partial vaporization of a once single phase liquid. Also in relation to nuclear reactor technology, dispersed flow in a batch process has applications to the design of the risers for boiling water reactors.

It will be seen from the literature survey that a good analysis of the gas-liquid batch bubbling process has been and still is needed. In the past twenty years, many analyses have been undertaken and experiments performed. This previous work has uncovered the existence of distinct

---

\*The phrase "stagnant liquid" implies a two-phase flow system with no liquid through-put.

flow regimes and has attempted to analyze each of these regimes in order to determine mathematical correlations that effectively describe what is experimentally observed. As the literature survey will indicate, however, still more data is needed to thoroughly describe the bubbling process in a batch system. This is particularly true in relation to the effect of  $L/D$  (i.e., the ratio of the height of the liquid column to the diameter of its cross section) on the bubbling process. Most of the previous experiments have been concerned with pipes of small diameter and, therefore, large  $L/D$ . Thus, a full understanding of the effect of small  $L/D$  which has important applications, some of which have been previously mentioned, has not yet been attained.

### 1.2 Review of Literature

From a review of some of the recent books by authors such as Brodkey [15], Wallis [3], and Govier [16], it is evident that there are several distinct bubbling regimes that can occur in a gas-liquid batch bubbling process. It is the purpose of this literature survey to introduce and discuss the previous work in relation to four of these regimes:

- a) the "ideal" or laminar regime

The bubbles are of uniform size and velocity and are uniformly distributed over the cross section of the flow. There is an absence of two-dimensional effects (such as bubble coalescence and turbulent convection currents), and

there is no interaction between the bubbles.

b) the "churn-turbulent" regime

This regime, which was first referred to as "churn-turbulent" by Zuber [8], is characterized by two-dimensional effects. There is large scale bubble interaction in the form of bubble coalescence and shattering. The cross section of the flow can be considered as two regions: a central core through which large spherical cap bubbles rise with liquid entrained in their wakes, and an annular region which is the result of the downward return flow of the liquid.

c) slug flow regime

The bubbles in this regime are spherical cap in shape with diameters of approximately that of the test section. As in the churn-turbulent flow, these bubbles entrain liquid in their wakes and transport it upward in a central core region while a return flow of liquid passes downward through the annulus.

d) pseudo-jet flow regime

This regime, which was referred to as "pseudo-jet" by Zuber and Findlay [14], is characterized by a collapsing annular flow. The liquid phase is primarily located next to the pipe wall in the form of an annulus while a two-phase mixture of gas and liquid droplets occupies the central core. This state is unstable, however, since the liquid flows downward in the annulus and eventually collapses into the air stream, which forces the liquid back to the wall. This

process is repeated over and over.

To achieve a basic understanding of any of these regimes, it is necessary to have a relation which compares the void fraction,  $\alpha$ , to measurable quantities. In the batch bubbling system these quantities include the properties of the fluid ( $\mu$ ,  $\rho_1$ ,  $\rho_2$ , and  $\sigma$ ), and the volumetric gas flow rate,  $Q_2$ , which will be expressed as the volumetric flux density<sup>\*</sup>,  $j_2$ :

$$j_2 = \frac{Q_2}{A} \quad (1)$$

where  $A$  is the cross sectional area of the flow.

Siemes [1] in 1954, noted the existence of two flow regimes and proposed the following relation between the volumetric flux density and the void fraction for a batch system<sup>\*\*</sup> operating in the laminar regime:

$$j_2 = u_t \alpha \quad (2)$$

where  $u_t$  is the velocity of rise of a single bubble in an infinite medium. This relation was presented as a first

---

<sup>\*</sup> The volumetric flux density was referred to as the "superficial velocity" in some earlier reports [2,8].

<sup>\*\*</sup> It should be noted since it will not be specifically stated every time that the remainder of the equations presented in this review deal only with batch bubbling systems unless stated otherwise.

approximation to his experimental data.

In 1961, Wallis [2] analyzed the bubbling of air through water and also arrived at the conclusion that there were two distinct flow regimes: the bubbly (i.e., laminar) and the slug flow regimes. In his paper [2] and in a later book [3], Wallis suggested the following relation for the bubbly regime:

$$j_2 = u_t \alpha (1 - \alpha) \quad (3)$$

Wallis [2] used essentially a heuristic argument to explain the form of this relation. He presented Equation (3) as the simplest relation that effectively described the behavior of  $j_2$  at the limiting conditions on  $\alpha$ , i.e., as  $\alpha$  approached zero and one. As  $\alpha$  approached zero, he assumed that the interaction between the bubbles was negligible, and thus  $j_2/\alpha$  was equal to the terminal velocity of rise of a bubble in an infinite medium. On the other hand, the situation as  $\alpha$  approached one was that of the drainage of a liquid through a foam when the foam was almost dry. In this case, the relative velocity between the liquid and the bubbles was very small, thus  $j_2$  was approximately equal to zero. (Equation (3) was first derived semi-empirically by Thornton [4] and his co-workers for liquid-liquid systems.)

Wallis [2,3] suggested the use of the expressions obtained by Peebles and Garber [5] for the terminal velocity

(refer to Appendix A) and, in particular, in his report [2] he expressed Equation (3) for bubbles in the size range of Region 4:

$$j_2 = 1.18 \left[ \frac{\sigma g (\rho_1 - \rho_2)}{\rho_1} \right]^{1/4} \alpha (1-\alpha) \quad (4)$$

The coefficient, 1.18, was revised by Harmathy [6] to 1.53, and more recently by Levich [7] to 1.41.

Zuber and Hench [8] derived an equation similar to Equation (3) for the laminar region but in a more general form:

$$j_2 = u_t \alpha (1-\alpha)^m \quad (5)$$

where  $m = 1, 3/4$ , or  $1/2$ , depending on the bubble size. Their analysis involved the balance between the lift and drag forces acting on a bubble in a swarm in order to obtain an expression for the relative velocity between the phases:

$$u_r = \left[ \frac{1}{C_D} \frac{4}{3} \right]^{1/2} \left[ \frac{g (\rho_1 - \rho_2) d}{\rho_1} \right]^{1/2} (1-\alpha)^{1/2} \quad (6)$$

The relation between the relative velocity and the volumetric flux density was given as

$$j_2 = \alpha u_r \quad (7)$$

Thus, by substituting for the drag coefficient in terms of the expressions obtained by Haberman and Morton [9], (refer to Appendix A), who also analyzed the problem of the terminal velocity of rise of different sized bubbles in an infinite medium, Zuber and Hench were able to arrive at the general relation (Equation (5)) for the laminar regime.

If the terminal velocity of Region 4 from Peebles and Garber [5], which corresponds to regions CD and DE of Haberman and Morton [9], is substituted into Equation (5), the following equation results:

$$j_2 = 1.18 \left[ \frac{\sigma g (\rho_1 - \rho_2)}{\rho_1^2} \right]^{1/4} \alpha (1-\alpha)^{1/2} \quad (8)$$

This equation differs from the correlation of Wallis [2,3], Equation (4), by a factor of 1/2 in the exponent of the  $(1-\alpha)$  term. The shape of Equation (8) can be viewed on Figure 1a.

This concludes the discussion of the literature in relation to the laminar bubbling regime. The churn-turbulent regime will be neglected for the moment and the slug flow regime considered next. The reason for this is that many earlier authors, with the exception of Zuber and Hench, failed to recognize the existence of a distinct regime separating

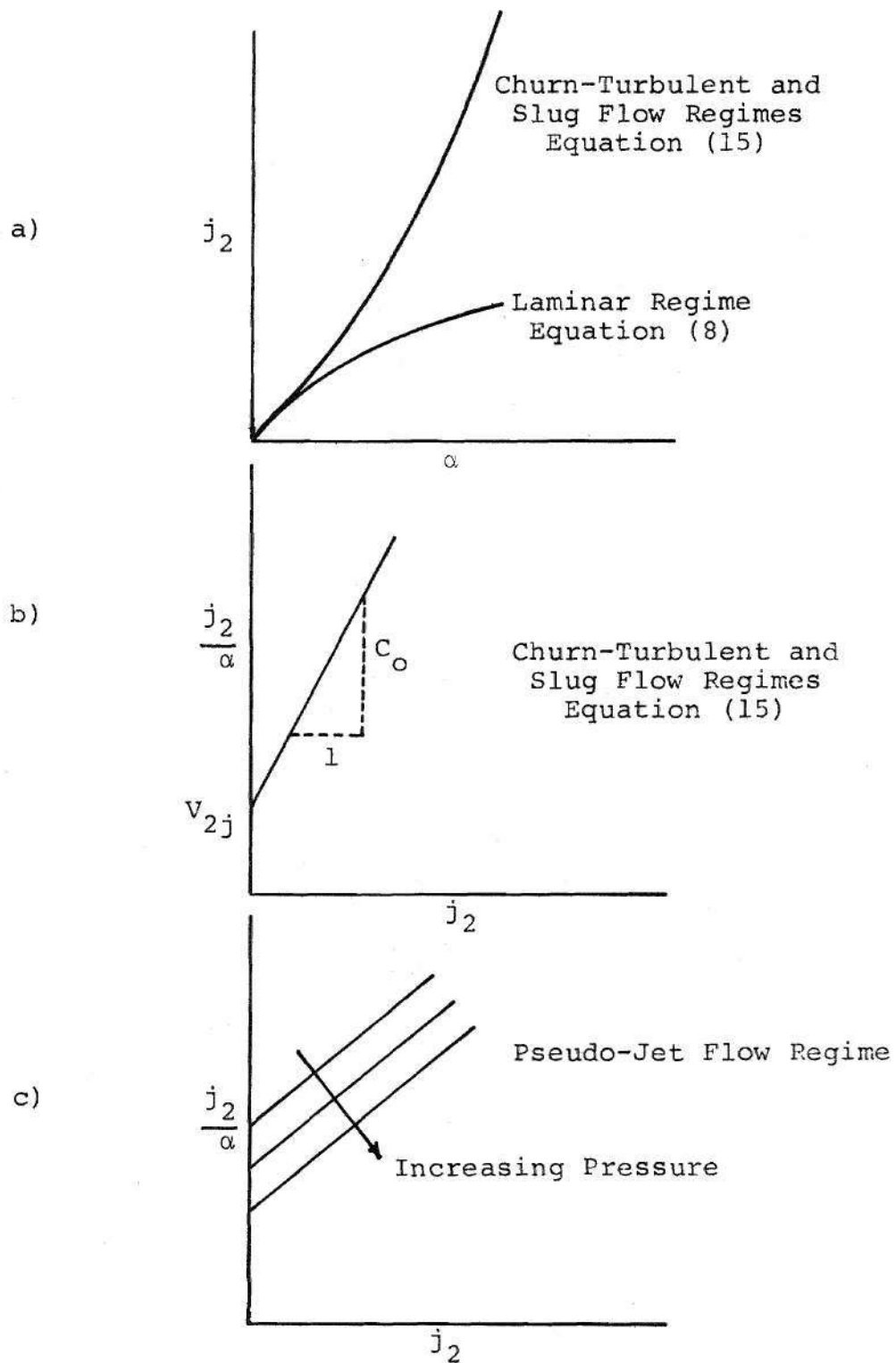


Figure 1. A Sample of the Graphs to be Used in the Analysis of the Data



the laminar from the slug flow regime. They referred to the separation as a "transition" region. It is true that a transition region occurs, but part of what they referred to as "transition" was in actuality the churn-turbulent regime. This regime was not detected by earlier authors because most of the experiments were performed on small diameter pipes (about 1 to 4 inches), and in such small pipes the terminal velocity of slugs and of spherical cap bubbles of Region 4 is very nearly the same. Thus, the churn-turbulent regime is difficult to observe.

Experimentation and analysis of the slug flow regime were presented by Nicklin [10] and Nicklin, Wilkes, and Davidson [11]. In general, they arrived at the following equation:

$$j_2 = u_t \frac{\alpha}{1 - C_0 \alpha} \quad (9)$$

where  $C_0$  accounted for non-uniform flow distribution and was taken equal to 1.2, and  $u_t$  was the terminal velocity of rise of a slug in a pipe of diameter slightly larger than that of the slug. Nicklin, Wilkes, and Davidson undertook experiments to determine  $u_t$  and arrived at the following conclusions:

a) slugs similar to the Dumitrescu-Taylor bubble, i.e., a wakeless slug, rise relative to the liquid ahead of them at a velocity

$$u_t = 0.35 (gD)^{1/2} \quad (10)$$

where D is the diameter of the pipe.

b) If there is no flow of liquid across any cross section ahead of a slug, slugs of all lengths rise at a velocity given by Equation (10).

Similar experiments for the determination of  $u_t$  were presented by Griffith and Wallis [12] and White and Beardmore [13], to name a few. They suggested equations of the form

$$u_t = C_1 (gD)^{1/2} \quad (11)$$

Griffith and Wallis plotted graphs of  $C_1$  versus  $Re_b$ , the Reynolds number based on the bubble, in order to determine a value for  $C_1$ , and White and Beardmore suggested the value 0.345.

In 1964, Zuber and Findlay [14] presented an analysis of two-phase flow that considered the effects of non-uniform flow, non-uniform concentration, and the local relative velocity on the average void fraction. They derived the following general relation, which was independent of flow regime and type of flow system (i.e., batch, cocurrent, or counter-current):

$$\left\langle \frac{j_2}{\alpha} \right\rangle = C_o \langle j_m \rangle + \left\langle \frac{\alpha V_{2j}}{\alpha} \right\rangle \quad (12)$$

where

$$j_m = j_1 + j_2 \quad (13)$$

was the volumetric flux density of the mixture, and

$$V_{2j} = v_2 - j_m \quad (14)$$

was defined as the drift velocity of phase 2. The coefficient,  $C_o$ , which was labeled the "distribution parameter" by Zuber and Findlay, accounted for the effect of the non-uniform velocity and concentration profiles. The value of  $C_o$  was determined from the exponents of the profile curves for established flows and was found to vary from 1.0 to 1.5 as the profiles varied from flat to parabolic. The last term of Equation (12) was referred to as the weighted average drift velocity and accounted for the effect of the local relative velocity and the concentration profile.

In their analysis, Zuber and Findlay noted that the simplest expression for the drift velocity was obtained by assuming that the drift velocity did not depend on the concentration, i.e., the presence of other particles. Thus,

the drift velocity and, consequently, the weighted average drift velocity were equal to the terminal velocity. For this case, the following general equation for the churn-turbulent and slug flow regimes in a batch system was obtained:

$$j_2 = u_t \frac{\alpha}{1 - C_o \alpha} \quad (15)$$

It can be seen from this equation that on a plot of  $j_2/\alpha$  versus  $j_2$  for each flow regime,  $C_o$  will be the slope of the resulting straight line and  $u_t$  the intercept with the  $j_2/\alpha$  axis. (Refer to Figure 1b, where  $V_{2j}=u_t$ ; Equation (15) is also shown on Figure 1a.)

The expressions suggested by Zuber and Findlay for the terminal velocities were the following:

a) for the churn-turbulent regime, the relation obtained by Harmathy [6] for Region 4:

$$u_t = 1.53 \left[ \frac{\sigma g (\rho_1 - \rho_2)}{\rho_1^2} \right]^{1/4} \quad (16)$$

b) for the slug flow regime, the following relation:

$$u_t = 0.35 \left[ \frac{g (\rho_1 - \rho_2) D}{\rho_1} \right]^{1/2}$$

where  $D$  was the diameter of the pipe. With the substitution of these terminal velocities, Equation (15) yielded for the slug flow and the churn-turbulent regimes, respectively:

$$j_2 = 0.35 \left[ \frac{gD(\rho_1 - \rho_2)}{\rho_1} \right]^{1/2} \frac{\alpha}{1 - C_o \alpha} \quad (18)$$

and

$$j_2 = 1.53 \left[ \frac{\sigma g(\rho_1 - \rho_2)}{\rho_1^2} \right]^{1/4} \frac{\alpha}{1 - C_o \alpha} \quad (19)$$

The pseudo-jet flow regime, which has been considered almost entirely in foreign literature, was analyzed by Zuber and Findlay [14]. By examining the results of several experiments which concerned steam-water mixtures in vertical containers of large diameter (which approximated the region above a reactor core), Zuber and Findlay noted that the data could be represented by straight lines with slopes, and thus, values of  $C_o$  between 1.15 and 1.25. These lines were pressure dependent in that an increase in pressure caused a parallel shift downward (as shown in Figure 1c). Zuber and Findlay suggested the following relation for this regime: (note that the intercept with the  $j_2/\alpha$  axis is dependent on  $\rho_2$ , the density of the gas, as opposed to  $\rho_1$  as in Equations (18) and

(19))

$$\frac{\langle j_2 \rangle}{\langle \alpha \rangle} = 1.2 \langle j_2 \rangle + A_p \left[ \frac{\sigma g (\rho_1 - \rho_2)}{\rho_2^2} \right]^{1/4} \quad (20)$$

where  $A_p$  was defined as

$$A_p = \frac{\langle \alpha V_2 j \rangle}{\langle \alpha \rangle} \left[ \frac{\rho_2^2}{\sigma g (\rho_1 - \rho_2)} \right]^{1/4} \quad (21)$$

The value of  $A_p$  for a given apparatus remained constant and independent of pressure. However,  $A_p$  was not constant for changes of system, such as changes of container geometry, liquid height, number, distribution, and size of the bubbling orifices.

In summary, it should be noted that, although mathematical correlations have been proposed for every regime and some experimentation has been used to support these formulations, the problem of bubbling of gases through liquids in batch systems is still not completely understood. More experimentation is needed to thoroughly describe the separate regimes in relation to characteristics, limits, predictability, and reaction to outside effects, such as L/D and the method of gas injection. Also, a more thorough analysis of the

pseudo-jet flow regime is needed.

### 1.3 Purpose

It is the purpose of this thesis to analyze the bubbling process in a batch system in order to attain a better understanding of the characteristics and limits of each flow regime, and to analyze the effect of L/D and plate porosity on the flow system in general. This thesis will be undertaken in order to lay a foundation for future work that will concern a more complete analysis of the pseudo-jet flow regime.

The method of attack for this thesis can be divided into three steps:

a) design and construction of the apparatus

The apparatus basically consists of two test sections in the form of vertical tubes, the inside diameters of which are 11.5 inches and 4.0 inches. The working fluids are air and water.

b) experimentation

Two porous plates (70 $\mu$  and 120 $\mu$ ) are used in conjunction with the 11.5 inch pipe and one plate (70 $\mu$ ) with the 4.0 inch pipe. The experiments consist of varying the air flow rate for each static height of water. Data is taken in order to calculate the void fraction.

c) correlation of the data

The data is analyzed in order to discover the dependence of void fraction on L/D, gas flow rate, and plate porosity.

## CHAPTER II

### EXPERIMENTATION

#### 2.1 Apparatus

The basic overall experimental apparatus consisted of two test sections seated on a six foot long table whose top was composed of three two-by-two foot sections of 3/4 inch plywood covered with formica. The largest of the test sections was constructed of three 52 inch long, 11.5 inch I.D., 12 inch O.D. plexiglass tubes arranged in a vertical fashion for a total height of 13 feet, as shown in Figure 2. The tubes were connected with aluminum flanges between which were rubber O-rings to prevent leakage. The bottom flange of the section of tube that rested on the table was designed with a center core that projected through the table, as shown in Figure 3, so that the air chamber could be attached or removed from beneath the table without disturbing the test section.

The air chamber consisted of an 11.5 inch O.D., 10.5 inch I.D. aluminum tube which was 14 inches in length. The top of this chamber was designed with a recessed lip 10.5 inches O.D. and 1/4 inch wide which allowed for the insertion of various thicknesses of porous plate up to 5/8 inch (see Figure 3). The plates were secured and sealed against air



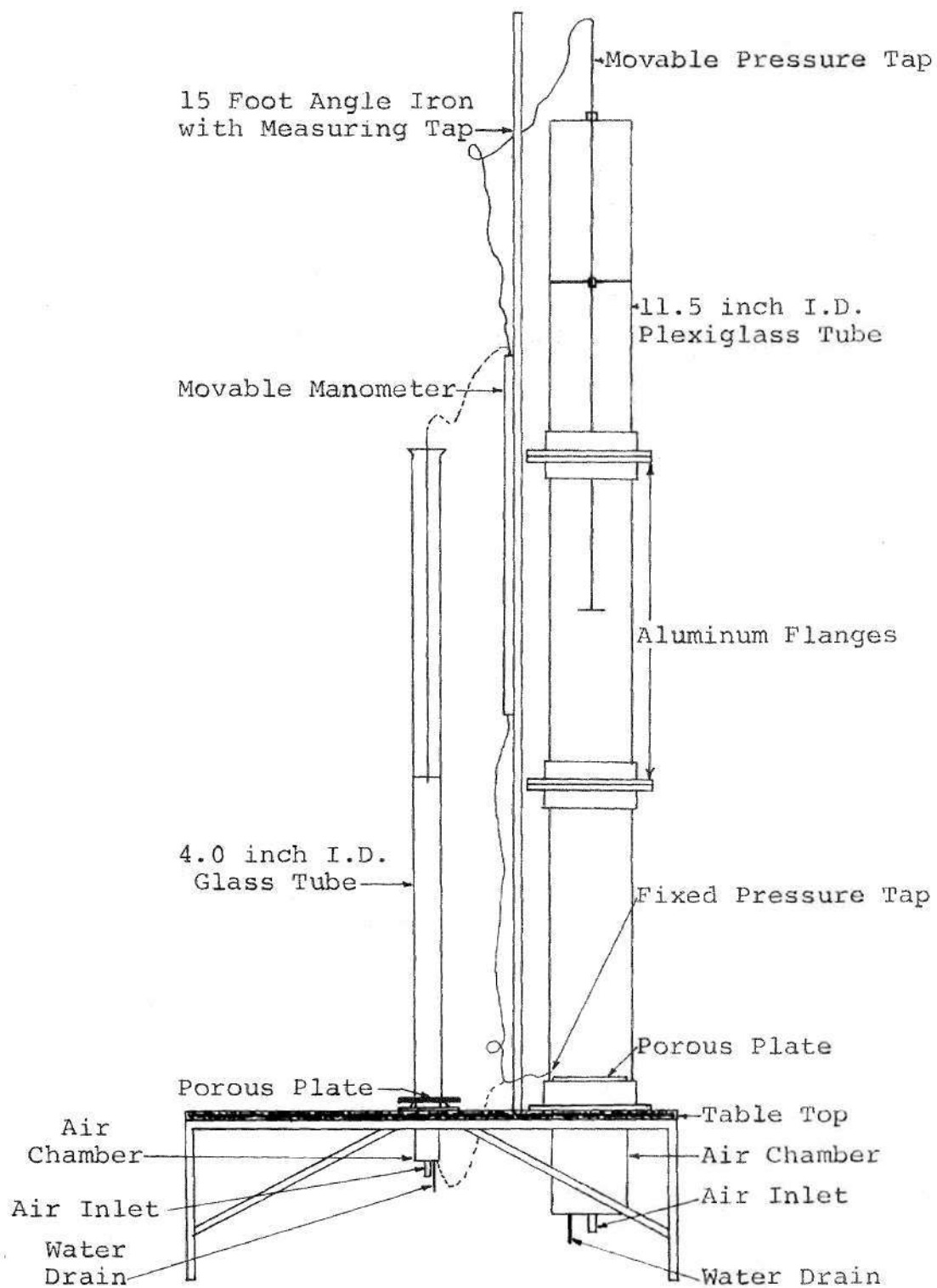


Figure 2. Overall View of Experimental Apparatus

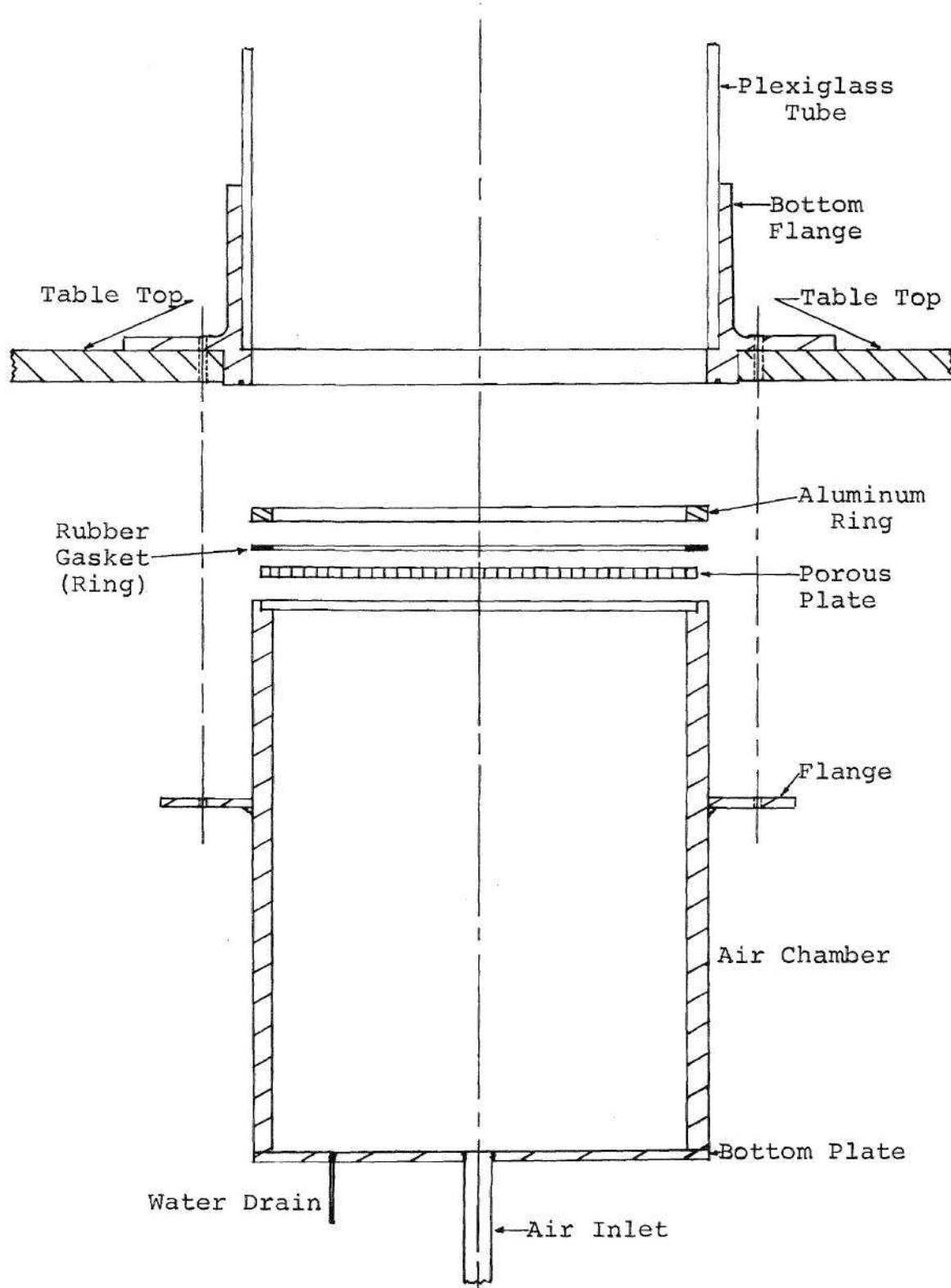


Figure 3. Cross Section of Air Chamber and Bottom Flange Assembly for the 11.5 Inch I.D. Test Section

leakage with an aluminum ring 11.5 inches O.D. and 10.5 inches I.D. and a rubber gasket of equal dimensions which were bolted at the top of the chamber. An aluminum flange 16 inches O.D. and 11.5 inches I.D. was welded 5 inches from the top of the chamber. This flange butted up against the projected part of the lower flange of the test section so that the air chamber was inserted into the test section a distance of 5 inches. The air chamber was designed in this way so that the porous plate was above the bottom flange of the test section and, thereby, could be easily viewed for the study of bubble formation. The bottom of the air chamber was a 1/4 inch thick aluminum plate through which projected a 3/4 inch I.D. pipe that acted as the air inlet and an 1/8 inch I.D. pipe which served as a water drain.

The second test section was a glass tube 4 inches I.D. and 8 feet in length. Its air chamber was an aluminum pipe 8 inches in length, 4 inches O.D., and 3.5 inches I.D., as shown in Figure 4. It was designed so that its flange, which was welded 2 inches from the top of the chamber, rested on the top of the table with the greater part of the chamber projecting through to the underside. The test section was slipped over the 2 inches of air chamber and rested on the flange, thereby necessitating the removal of the glass tube in order to change the porous plate.

The top of the air chamber was designed with a cover much like that used on a fruit jar. The cover was 4 inches

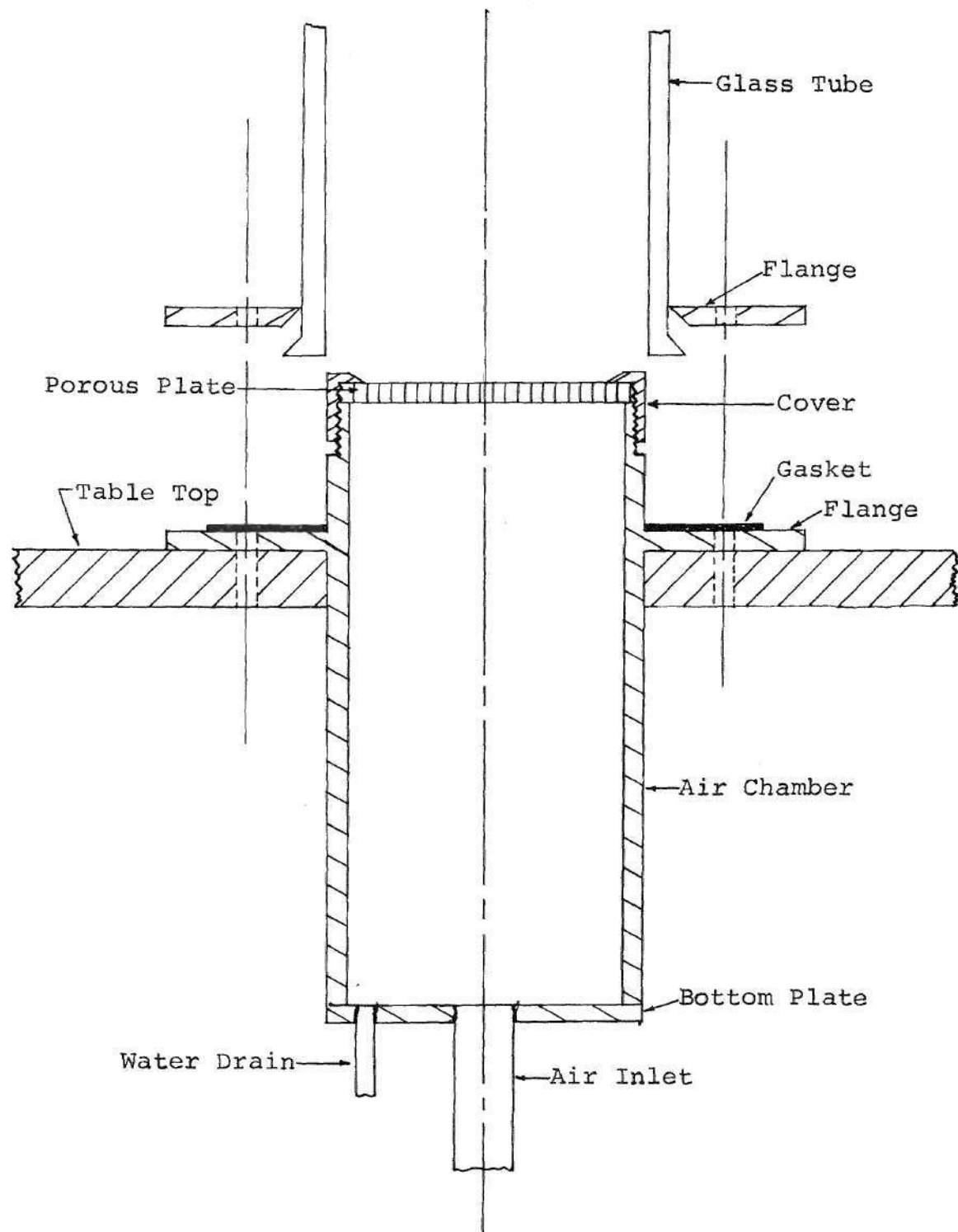


Figure 4. Cross Section of Air Chamber and Lower Assembly for the 4.0 Inch I.D. Test Section

in diameter and the hole in its center was 3.5 inches in diameter. A porous plate was fitted into the cover which was screwed down tight to prevent leakage of air around the plate.

Two porous plates were used in the experiments and their porosities were 70 and 120 $\mu$ . The thicknesses of the plates were 5/8 inch for the 120 $\mu$  and 3/8 inch for the 70 $\mu$ .

## 2.2 Instrumentation

The air flow rates were measured by means of two flowmeters (rotameters) whose ranges were 1.8 to 18 cfm and 5 to 50 cfm. Pressure gauges were used to measure the exit pressure of the flowmeters and a thermometer was used to measure the temperature of the air flowing through the flowmeters. The exit pressure and temperature readings were required in order to calculate a correction factor for the flowmeters, since their scales were calibrated for an exit pressure and temperature of 14.7 psia and 70°F. (See Appendix B.)

During experimentation it was difficult to obtain steady flowmeter readings. Generally, the fluctuations experienced by the low range flowmeter were no more than 0.4 cfm in magnitude. However, for use with the 4 inch I.D. test section, they could become as high as 2 cfm. The high range flowmeter fluctuated about 3 cfm at large values of cfm and was, for the most part, steady at low values.

Between the two test sections, there was a 15 foot

vertical piece of angle iron to which was attached a measuring tape. On the side of this angle iron there was a movable manometer in the form of a glass tube 8 mm in diameter and 4 feet in length. This manometer could be adjusted to allow for the range of readings associated with any static height of water. It was used to measure void fraction by reading the difference between two pressure taps:

a) fixed tap

A fixed tap was located at the bottom of each test section. For the 11.5 inch I.D. test section, the pressure tap was inserted through the wall of the plexiglass tube just above the porous plate. The fixed tap for the 4 inch I.D. test section passed up through the air chamber and projected through the porous plate. A plastic hose was used to connect the pressure tap to the bottom of the manometer. This hose was filled with water and care was taken to insure that no bubbles were admitted to the hose.

b) movable tap

The movable tap or, more correctly, pressure probe consisted of one, two, or three 4 foot sections (depending on the height of the water) of 8 mm glass tubing connected with short pieces of rubber tubing. At each rubber joint in the probe there was a "cross" made of small diameter plexiglass rod. This "cross" was used to keep the glass tubing away from the sides and approximately in the center of the test section. The probe was suspended at the top of each test

section and extended downward into the liquid. For the 11.5 inch I.D. test section, the end of the probe was an inverted T, while for the 4 inch tube, it was a straight pipe. The inverted T was used to obtain an average value of the pressure across the cross section. The T, however, was too large for the 4 inch I.D. test section so the straight pipe was used. The tap was connected to the manometer by means of a plastic hose that was "pressurized" with a small amount of air from the main supply so that bubbles were admitted very slowly from the tap into the liquid.

Two readings were taken from the manometer for the calculation of the void fraction. The first reading,  $h_1$ , was recorded with the main air supply off (i.e., with no reading on the flowmeters), and with the movable tap just under the surface of the water and pressurized so that it bubbled slowly. When the main air was turned on and increased, the volume of the water in the test section expanded and the level in the manometer fell. For a given air flow rate, the second reading was taken from the manometer and subtracted from the first to give a  $\Delta h$ , which was proportional to the pressure of the water above the movable tap. But the water above the movable tap was equal to the water displaced by the bubbles below the tap, so the void fraction was calculated by

$$\alpha = \frac{\Delta h}{h_1} \quad (22)$$

(The void fraction can also be measured from the ratio of the volume expansion to the final volume of the liquid column.)

When the main air supply was on and the experimentation was in progress, the level of the water in the manometer was always fluctuating. These fluctuations ranged from 1/2 inch for bubbling in the laminar regime to as much as 2 inches for the transition. In the churn-turbulent and slug flow regimes, they were never more than 1 inch. Generally, the motion of the level in the manometer was of a regular nature for the laminar, churn-turbulent, slug, and pseudo-jet flow regimes, but was very erratic for the transition region. Thus, a long observation time was required to obtain an average value of  $\Delta h$  for the transition region.

### 2.3 Experimental Procedure

The experimental procedure can best be described in two general categories: set up and experimentation.

#### a) set-up

The barometric pressure and supply air temperature were recorded. The test section was filled with water to the desired level, while a very slight bubbling was maintained from the porous plate in order to prevent seepage of the water into the air chamber. The movable tap was adjusted so that it was just under the surface of the water and then pressurized so that it bubbled very slowly. At this point,



the first reading,  $h_1$ , was taken from the manometer. The porous plate was "cleared" by forcing air from the main supply through the porous plate at the maximum flow rate. The "clearing" process was needed in order to drive the water from all the pores in the porous plate. This process was characterized by a continual drop in the exit pressure of the flowmeter for a constant air flow rate. When the pressure reading stabilized, the "clearing" process was complete.

b) experimentation

Various flow rates were maintained while the readings of pressure and manometer level were recorded. The "visual height", which was the height of the surface of the water in the test section, was also recorded. This was used to check the volume expansion and thereby the void fraction.

For the 11.5 inch I.D. test section, a "run" for a given height of water consisted of the recording of data for decreasing flow rates from 50 to 15 cfm in intervals of 5 cfm for the upper range flowmeter, and from 10 to 1.8 cfm in intervals of 1 cfm (with exception of the interval from 3 to 1.8 cfm) for the lower range flowmeter. The data for the 4 inch I.D. test section was taken for increasing flowmeter readings from 2 to 18 cfm in intervals of 2 cfm on the low range flowmeter and from 20 to 25 cfm using the interval of 5 cfm on the upper range meter, where applicable. For the static heights of water of 1 and 2 feet, 25 cfm was used as the maximum value, but for 3 and 4 feet, problems arose

concerning overflow due to the limiting height of the test section. The maximum flow rate for 3 feet was 16 cfm, and that for 4 feet was 8 cfm.

After each set of "runs", which consisted of static heights of 1 through 8 feet for the 11.5 inch I.D. test section and 1 through 4 feet for the 4 inch I.D. tube for one porous plate, the test section was drained, the air chamber removed, and the plate replaced with one of different porosity. The air chamber was then reinserted, the test section refilled, and experimental procedure restarted.

The experimental data is tabulated in Appendix C.

## CHAPTER III

## RESULTS AND DISCUSSION

The results obtained from the experiments can best be exhibited on graphs of  $j_2$  versus  $\alpha$  as shown on Figures 5, 6, and 7. From these graphs the relationship between  $j_2$ , the independent variable in the experiments, and  $\alpha$ , the dependent variable, can be analyzed. From Figures 5 and 6, on which is presented the data for the 11.5 inch test section, it can be seen that the bubbly flow passes through three distinct regimes: the laminar, transition, and churn-turbulent regimes. What is not evident is that a fourth regime, the slug flow regime, is also present (as will be shown later). From Figure 7, which is the data for the 4 inch I.D. test section, it is not quite as easy to determine which flow regimes are present. There appears to be two regimes: the slug flow regime and the collapsing annular flow, or pseudo-jet flow regime. The churn-turbulent regime may be present but it is very hard to detect (as previously discussed).

Since the data is so conveniently divided into distinct regimes, it will be easiest to analyze each regime separately in their order of occurrence with increasing volumetric flow rate. For each regime, a description based on experimental observation will be presented, along with a

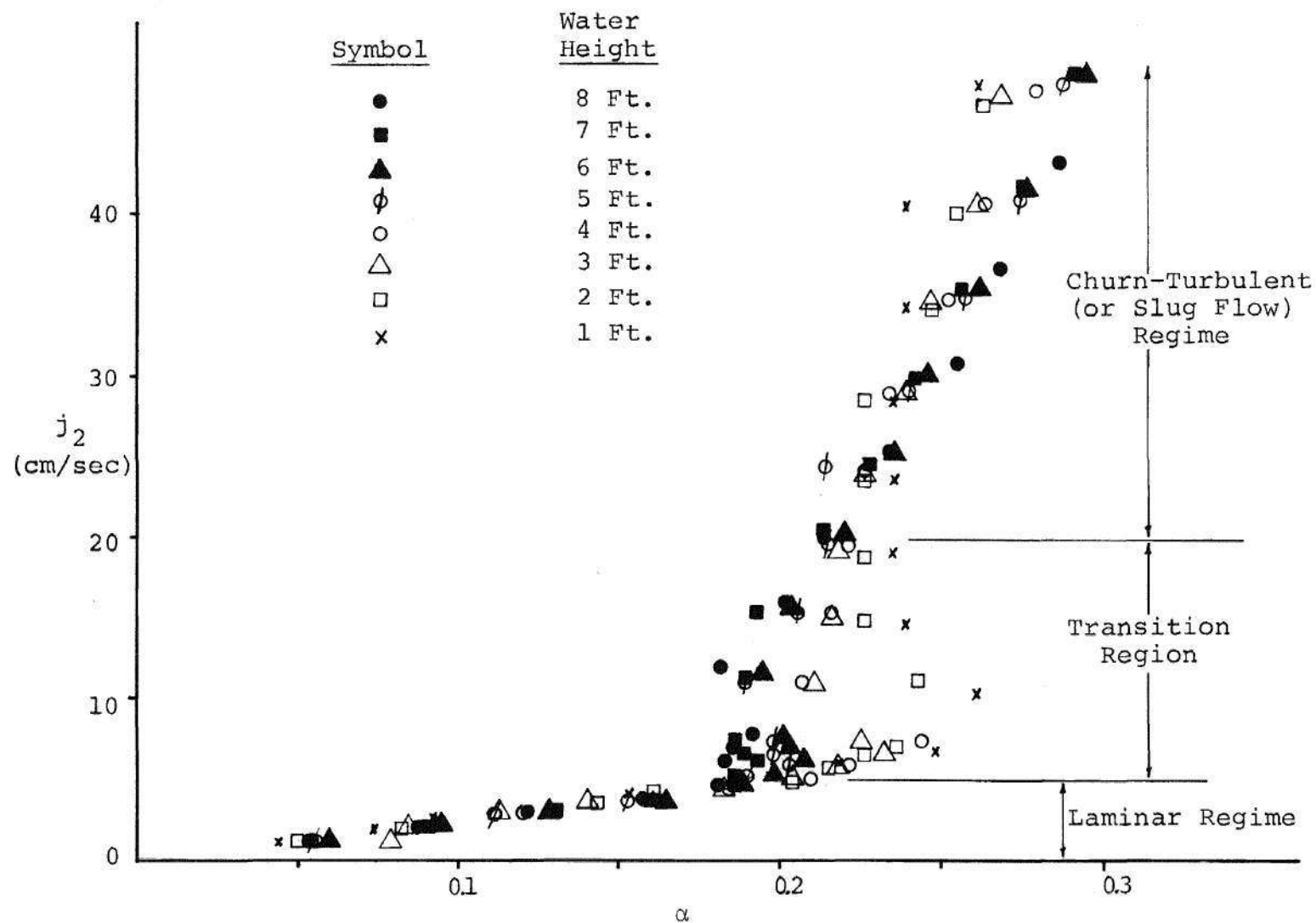


Figure 5. Volumetric Flux Density Versus Void Fraction for the 11.5 inch I.D. Test Section Using the 120 $\mu$  Porous Plate

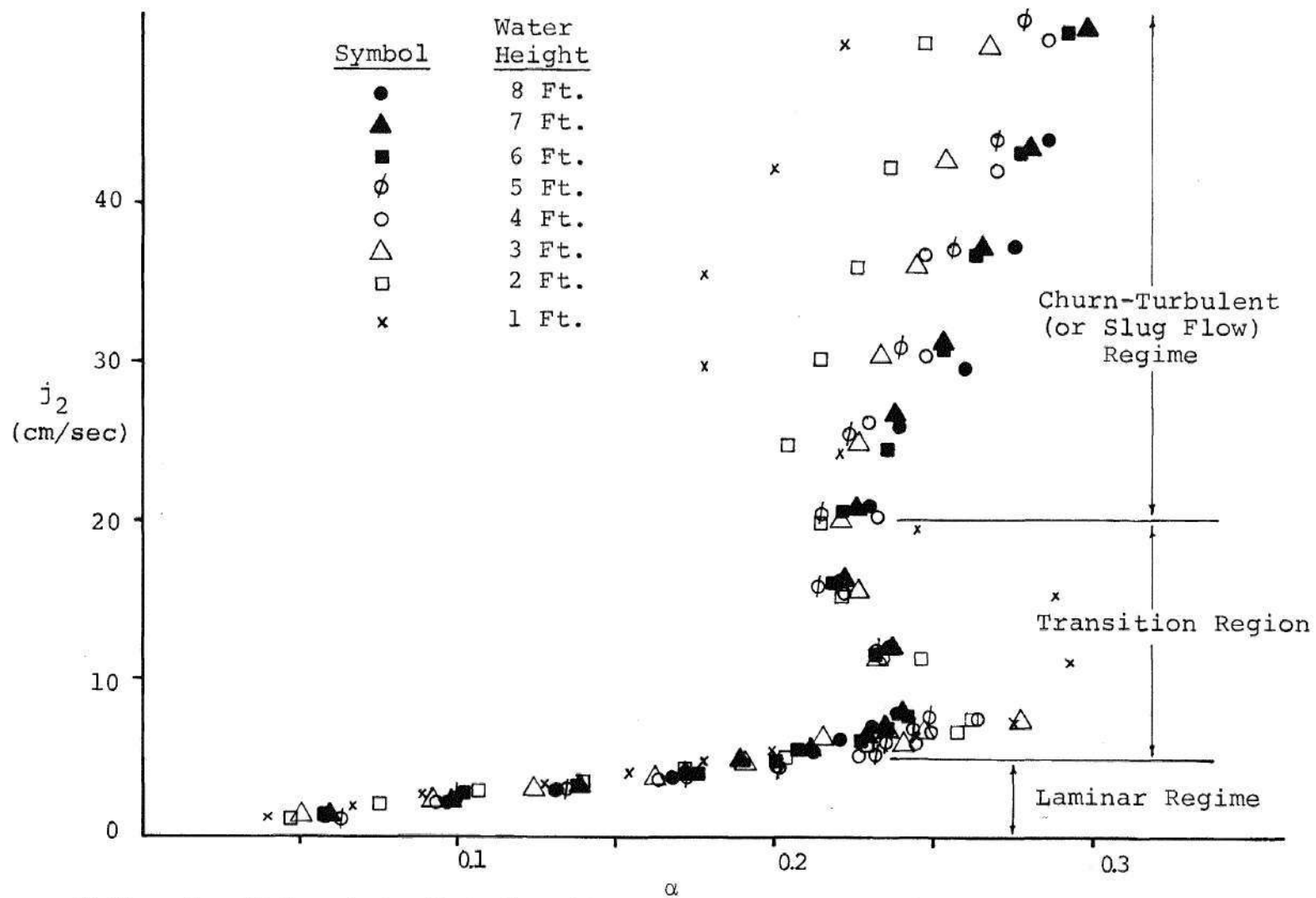


Figure 6. Volumetric Flux Density Versus Void Fraction for the 11.5 inch I.D. Test Section Using the 70 $\mu$  Porous Plate

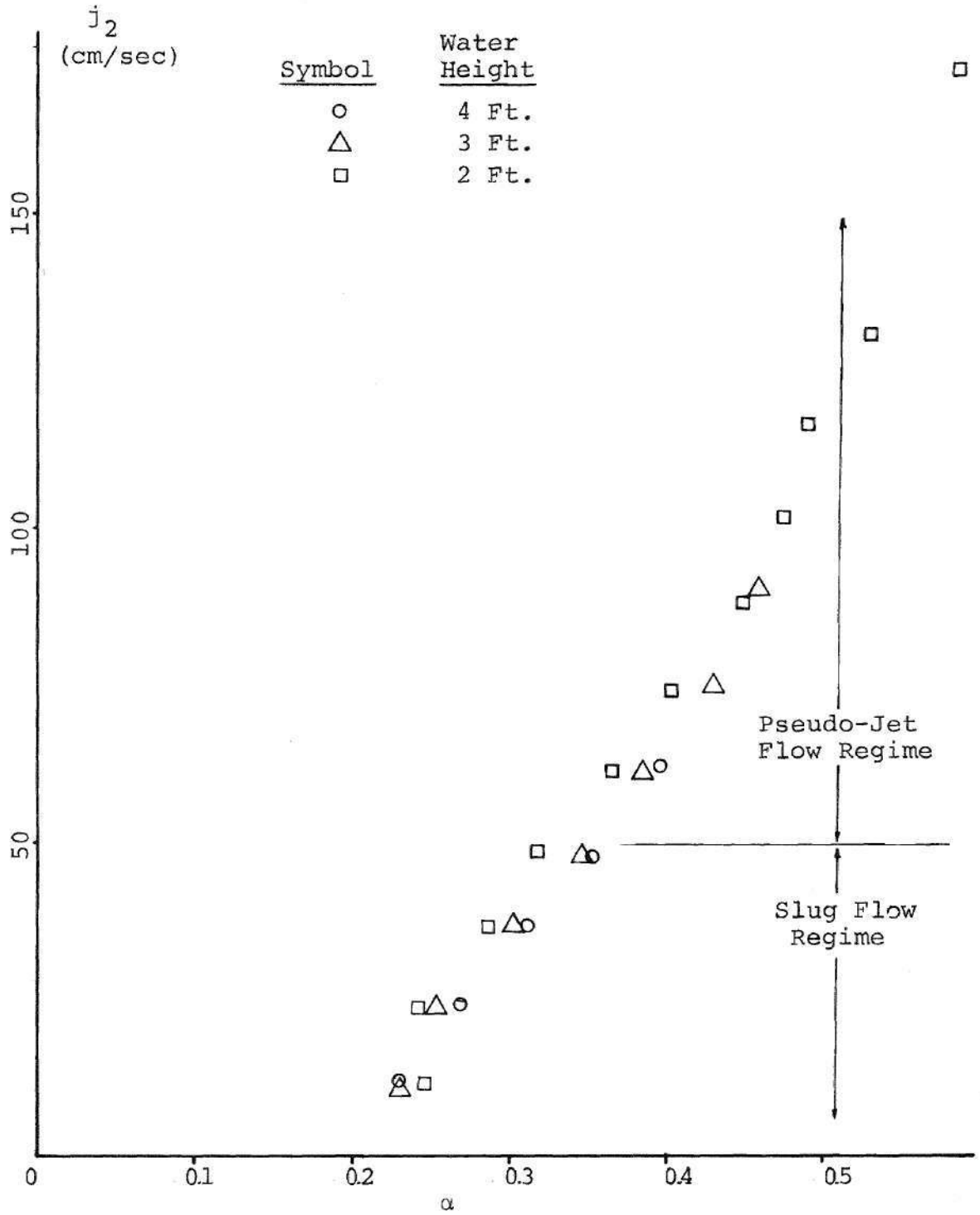


Figure 7. Volumetric Flux Density Versus Void Fraction for the 4.0 Inch I.D. Test Section

discussion of the results.

a) laminar bubbling regime

From the data obtained using the 11.5 inch I.D. test section, this regime was found to exist for values of  $\alpha$  between 0 and 0.20, and  $j_2$  between 0 and 5 cm/sec. The laminar bubbling regime was not observed in the 4 inch I.D. test section because of the limitations of the flowmeters, which could attain a low value of only 1.8 cfm ( $j_2=11$  cm/sec for the 4 inch pipe).

The laminar region was characterized by uniformly sized and shaped bubbles (i.e., oblate spheroids with diameters of about 0.55 cm), uniformly distributed across the cross section and rising with uniform velocity. There were no bubble interactions in the form of coalescence or shattering and there were no convection currents. In fact, there was very little liquid motion at all. This type of flow was not experienced in the entire length of the tube, however; the "true" laminar bubbling regime occurred only after an "entrance region" of about two feet. This "entrance region," which was caused by the non-uniform effects of the porous plate, was characterized by a swirling motion of the bubbly flow much like tornado clouds. With this observation in mind, it should be noted that for static water heights of 1 and 2 feet, the non-uniform effects were never dissipated and, thus, the laminar regime, as described above, never truly occurred.

From Figures 5 and 6, it is evident that in the laminar

regime the void fraction increases very rapidly with increasing volumetric flux density and is independent of  $L/D$  and plate porosity. (The lack of dependence of the void fraction on plate porosity was observed by comparing Figures 5 and 6. This is not conclusive evidence, however, since in the first place only two different plates were used, and in the second, it became obvious when the method of rating these plates was explored that the difference in these porosities was not very substantial. The plate porosity was determined by the manufacturer by considering the average value over a given area; thus a plate with a porosity of  $70\mu$  could have pores ranging in size from  $35\mu$  to  $120\mu$ .) It also appears from Figures 5 and 6 that the data for the laminar region can be represented as a straight line. To explore this possibility, Figures 8 and 9 will be considered.

Figures 8 and 9 give an expanded view of the laminar and transition regimes. The straight line fit to the data can be considered as the correlation suggested by Siemes [1] in Equation (2) (this is shown as the solid line). Thus, the slope of this line, 24 cm/sec, is the terminal velocity of rise of a single bubble. This value agrees quite well with the terminal velocity of a bubble as determined from the graph of Haberman and Morton [6] (see Appendix A) for bubble of diameter 0.55 cm; from the graph,  $u_t$  equals 25 cm/sec. This bubble diameter of 0.55 cm corresponds to region DE of Haberman and Morton, and Region 4 of Peebles



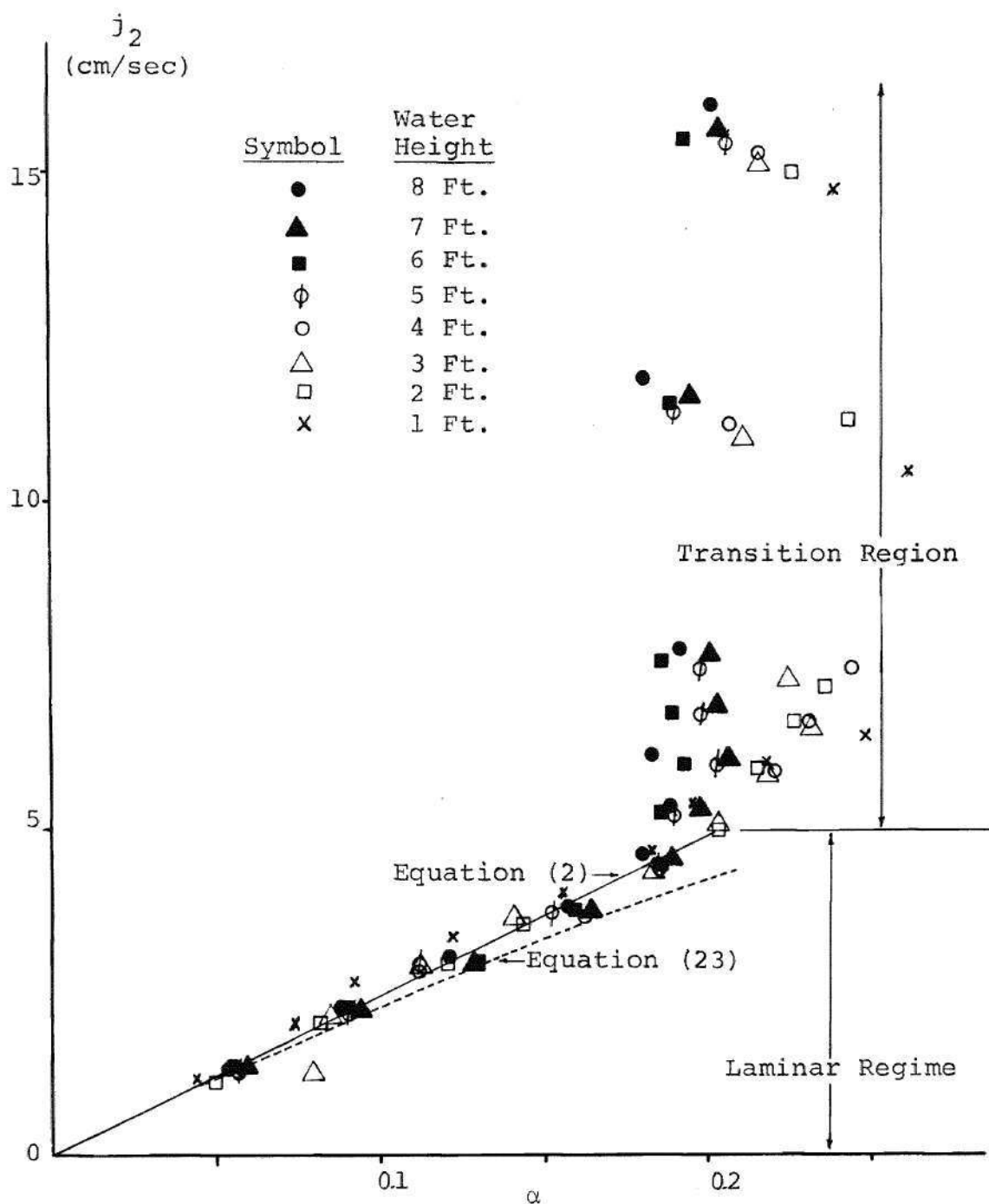


Figure 8. Volumetric Flux Density Versus Void Fraction for 11.5 inch I.D. Test Section Using the 70 $\mu$  Porous Plate

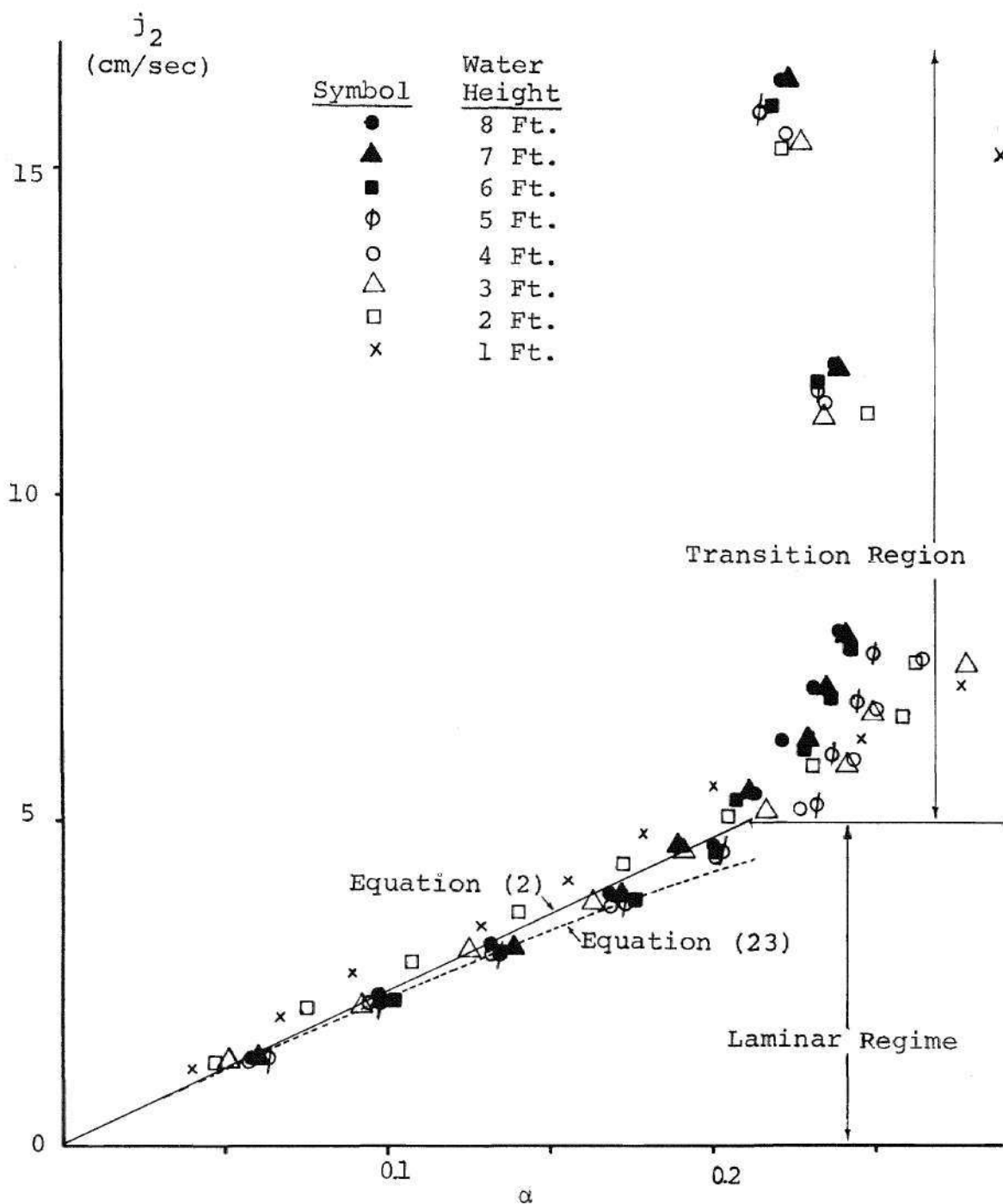


Figure 9. Volumetric Flux Density Versus Void Fraction for the 11.5 Inch I.D. Test Section Using the 120 $\mu$  Porous Plate

and Garber [5]. For these regions of bubble size, Zuber and Hench [1] suggested the equation

$$j_2 = u_t \alpha (1-\alpha)^{1/2} \quad (23)$$

which is Equation (5) with  $m$  equal to  $1/2$ . Equation (23) with  $u_t$  equal to 24 cm/sec, is plotted as the dotted line on Figures 8 and 9. It can be seen (particularly for Figure 9), that either curve is a possible fit to the data. In order to determine which correlation is the more accurate, a closer look at the laminar regime will be needed.

Figures 10 through 15 are plots of  $j_2$  versus  $\alpha$  for the laminar region. Figures 10, 12, and 14 deal with the static water heights of 2, 5, and 7 feet, respectively, for the 70 $\mu$  porous plate; and Figures 11, 13, and 15 consider the heights of 4, 6, and 8 feet for the 120 $\mu$  plate. The dotted line on each figure represents Equation (23) with  $u_t$  taken as the slope of the straight line drawn through each set of points. It is obvious from these figures that the straight line is the better approximation to the data. It should also be noted that the terminal velocity for each height of water, as determined from Figures 10 through 15, is not the same but varies from about 22 to 25 cm/sec. It may first be assumed that this shifting of the data line is due to the effect of  $L/D$ . This is not the case, however, since an examination of

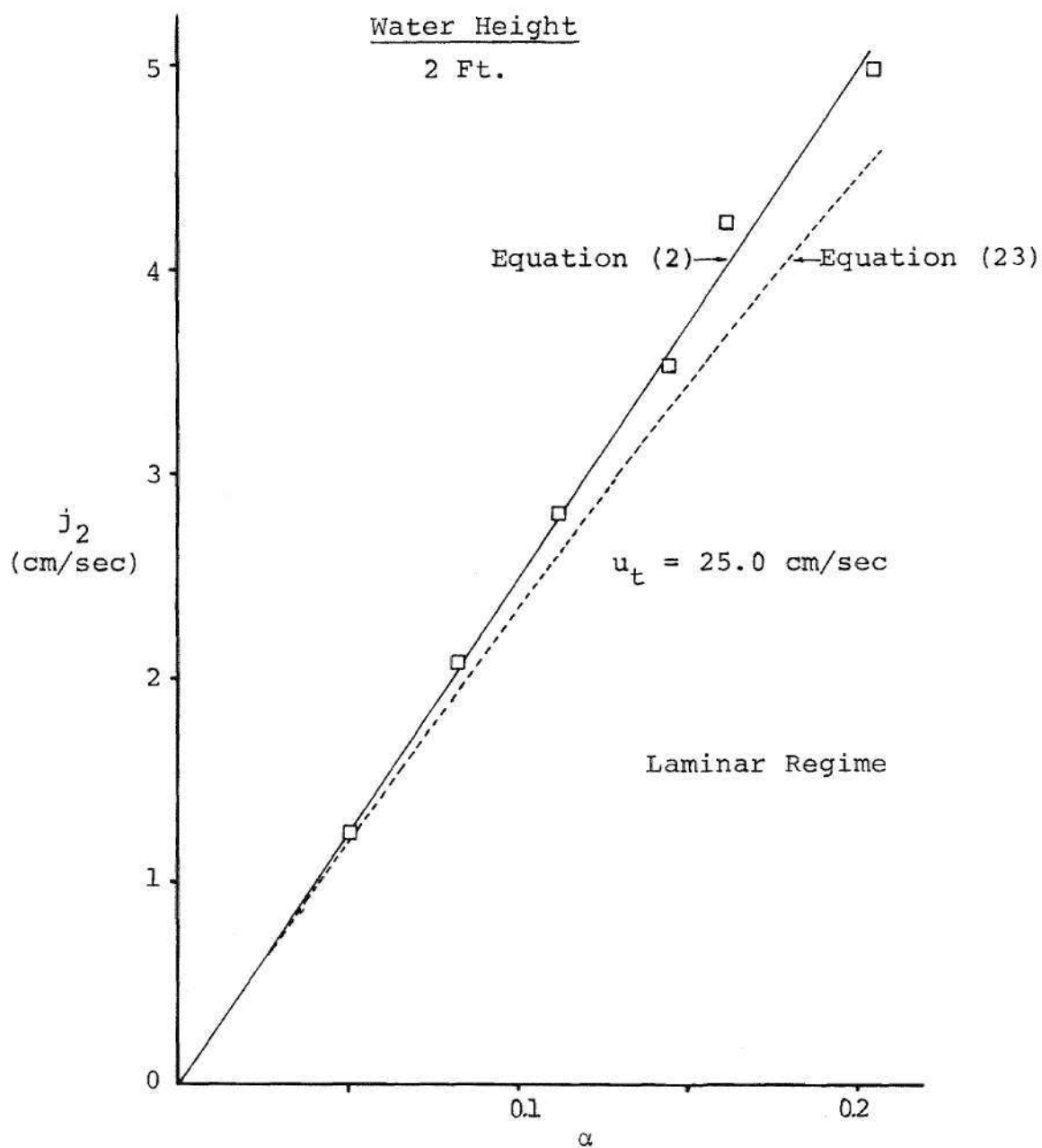


Figure 10. Volumetric Flux Density Versus Void Fraction for the 11.5 Inch I.D. Test Section Using the 70 $\mu$  Porous Plate

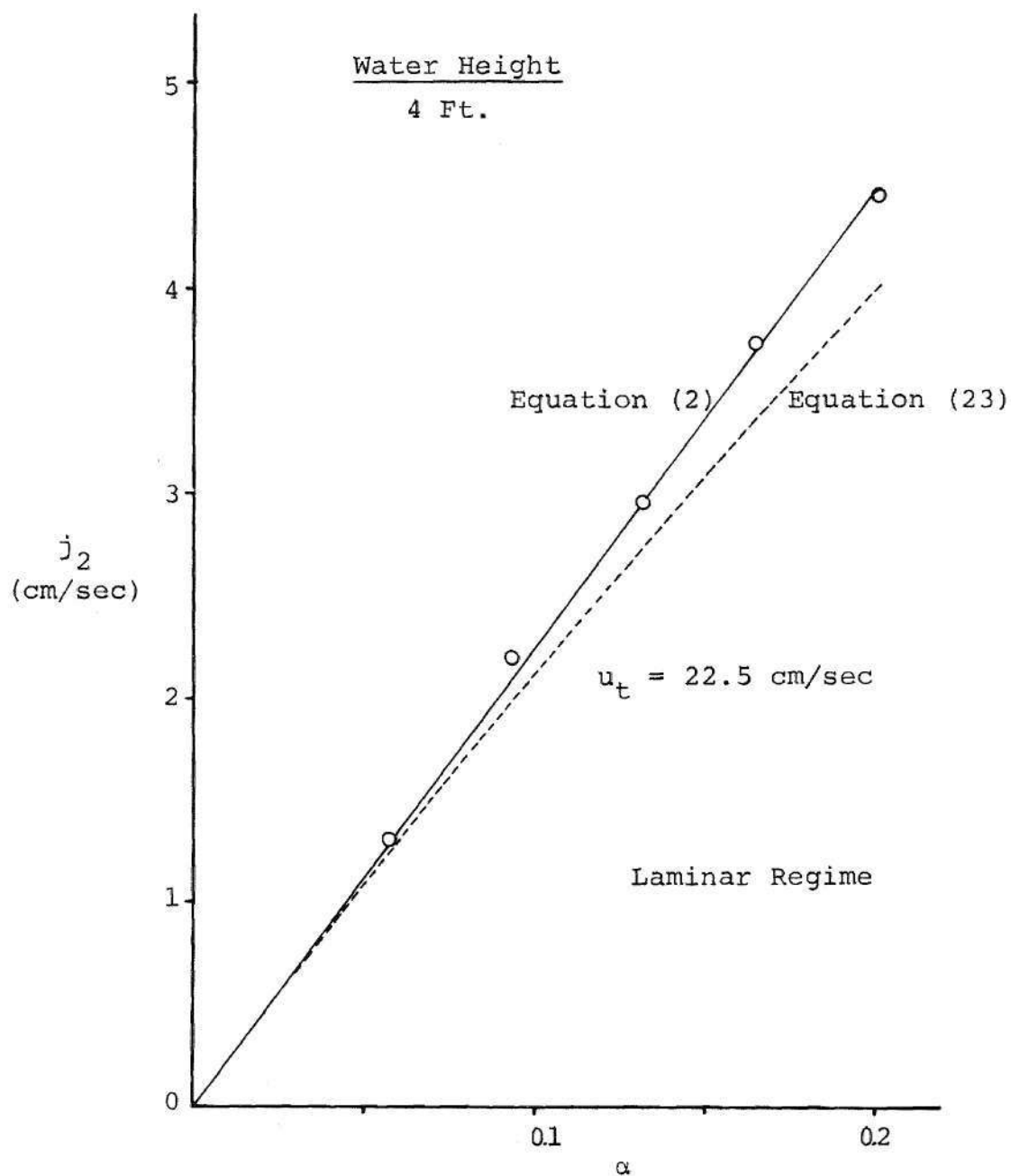


Figure 11. Volumetric Flux Density Versus Void Fraction for the 11.5 Inch I.D. Test Section Using the 120 $\mu$  Porous Plate

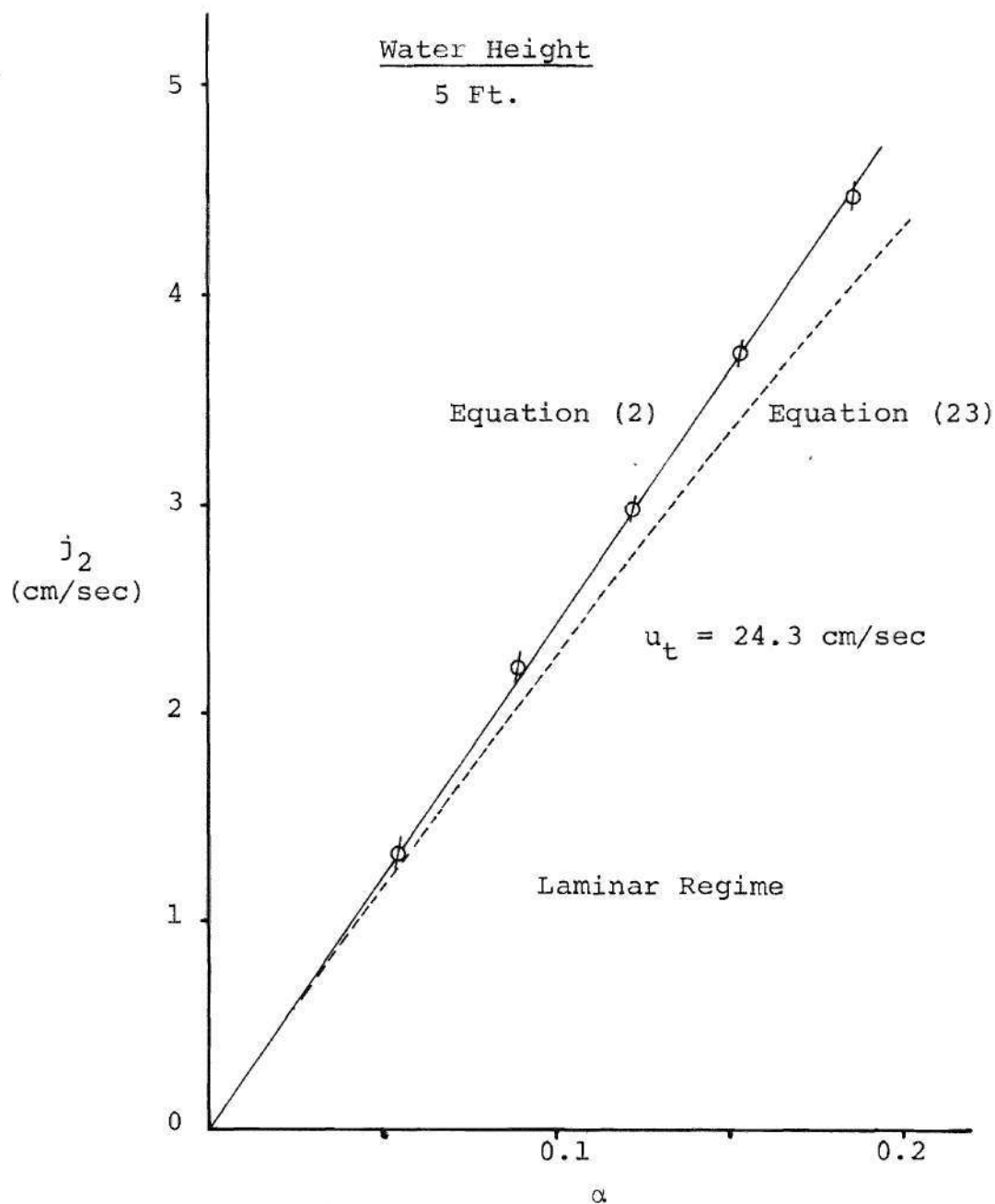


Figure 12. Volumetric Flux Density Versus Void Fraction for the 11.5 Inch I.D. Test Section Using the 70 $\mu$  Porous Plate

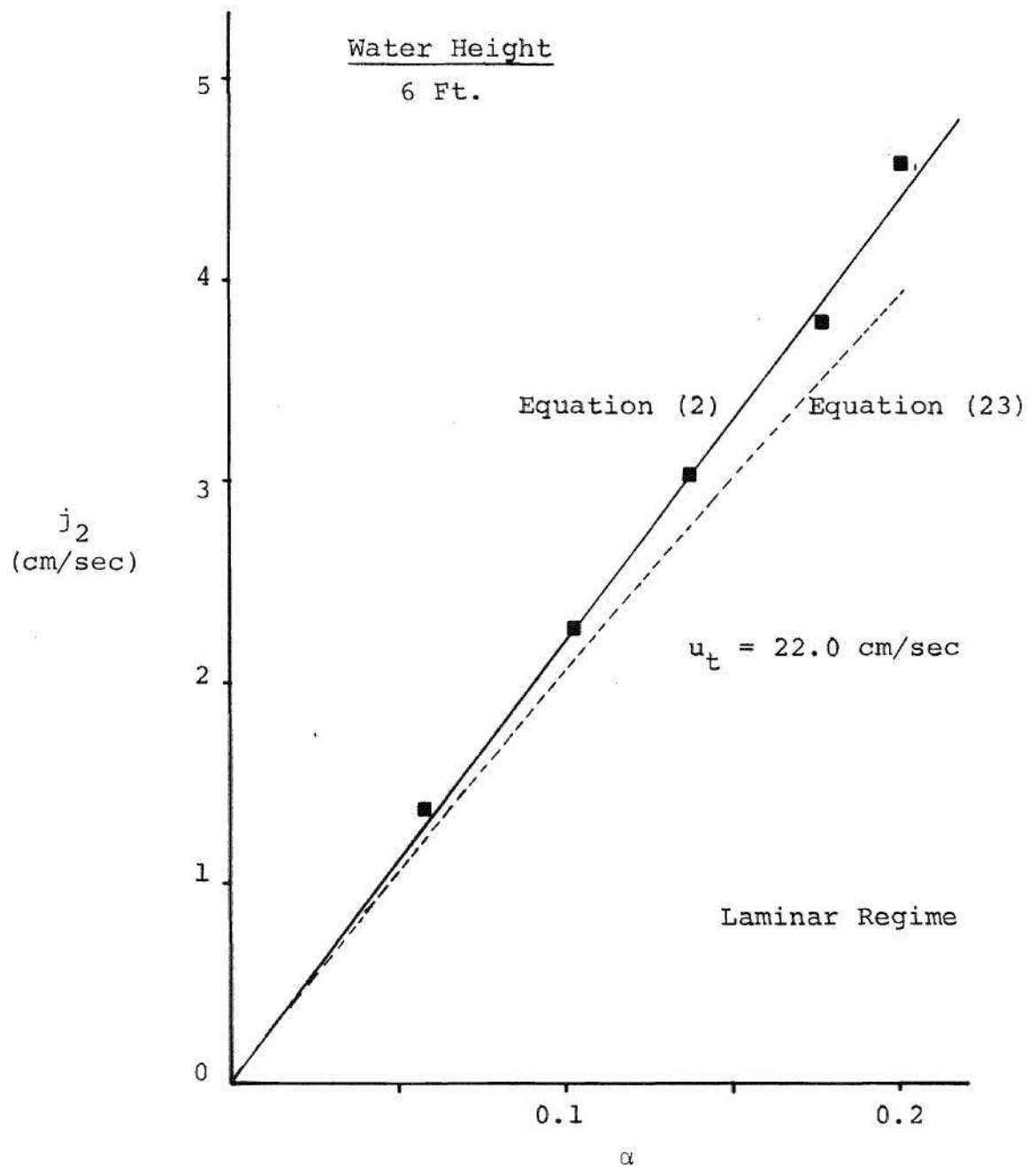


Figure 13. Volumetric Flux Density Versus Void Fraction for the 11.5 Inch I.D. Test Section Using the 120 $\mu$  Porous Plate

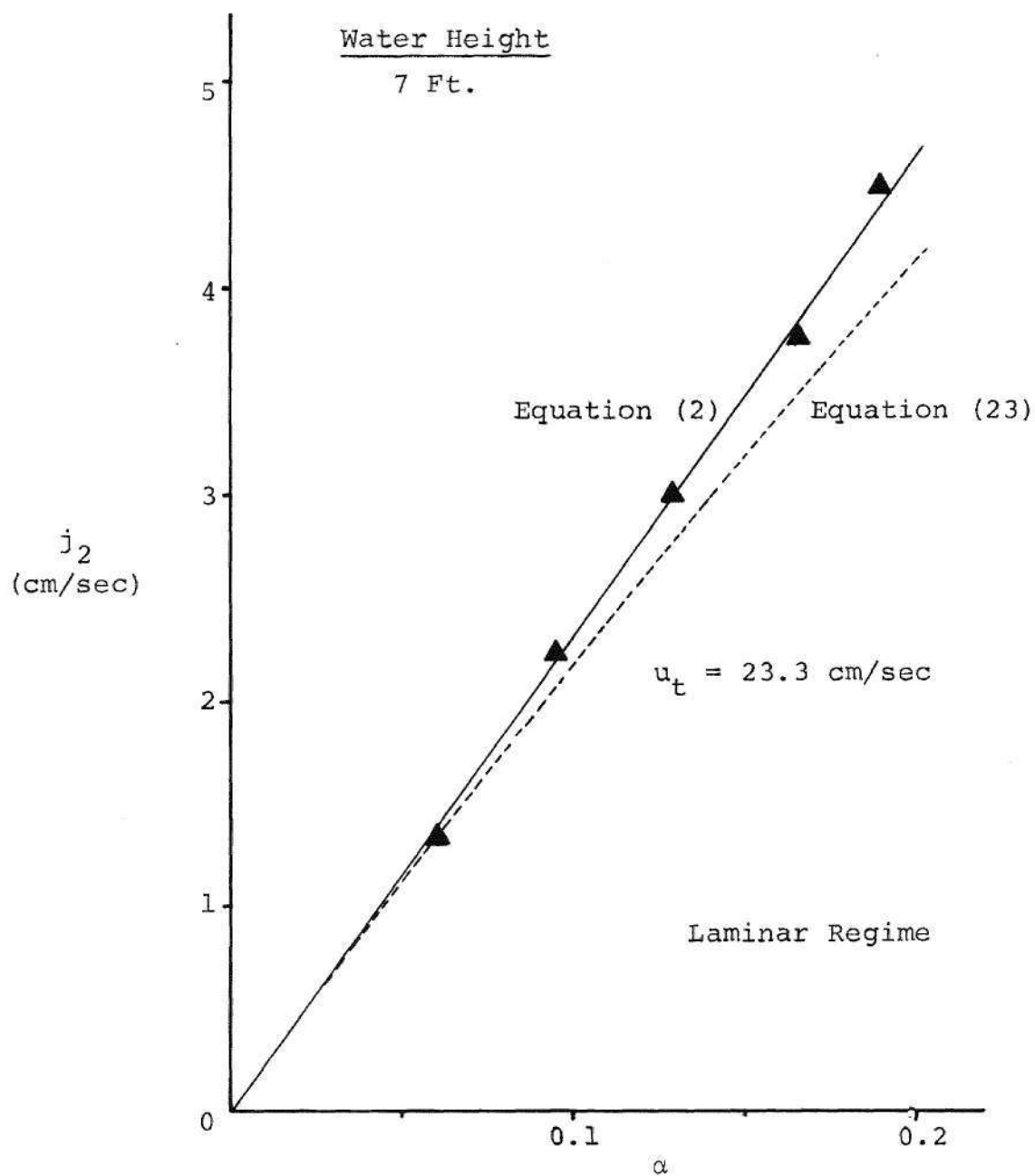


Figure 14. Volumetric Flux Density Versus Void Fraction for the 11.5 Inch I.D. Test Section Using the 70 $\mu$  Porous Plate



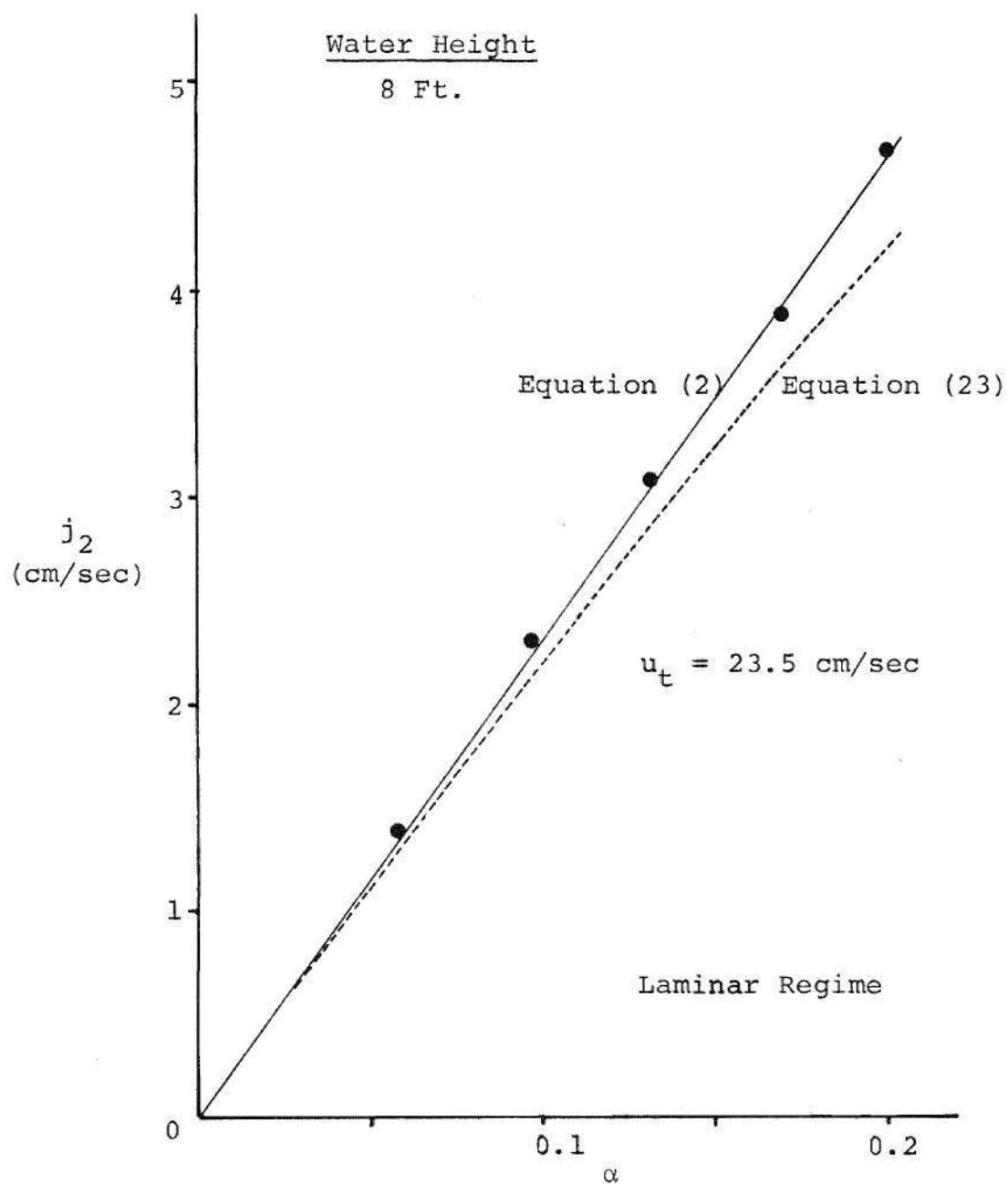


Figure 15. Volumetric Flux Density Versus Void Fraction for the 11.5 Inch I.D. Test Section Using the 120 $\mu$  Porous Plate

the figures reveals that the variation of slope with  $L/D$  does not follow a regular pattern as it does in other regimes (as will be shown later). For the purpose of predicting the laminar bubbling regime, this difference between 22 and 25 cm/sec for the terminal velocity is not crucial.

b) transition region

The beginning of this region was evident because of the presence of an occasional large bubble rising through the otherwise laminar bubbly flow. These few large bubbles were the result of coalescence since no large bubbles were formed at the surface of the porous plate. As the air flow was increased, however, large bubbles of the spherical cap variety began to form near the plate. These bubbles were of non-uniform size and generated wakes as they rose. There was obvious bubble interaction in the form of coalescence and shattering.

As shown in Figures 5 and 6, the range of this region extends from  $j_2$  approximately equal to 5 cm/sec to about 20 cm/sec, and the net increase in  $\alpha$  is about 0.02 (from 0.20 to 0.22). The void fraction first increases and then decreases with increasing  $j_2$  in what could be described as an S-fashion. It is noted that for values of  $j_2$  up to about 11 cm/sec, the void fraction increases at constant  $j_2$  for decreasing  $L/D$  (which varies from 8.35 to 1.04). As  $j_2$  increases above 11 cm/sec, however, the spread of the data due to  $L/D$  decreases and, in fact, the effect of  $L/D$  on  $\alpha$  begins

to reverse. During this reversal, the flow changes to the churn-turbulent regime. It is also interesting to note that on plots of  $j_2/\alpha$  versus  $j_2$  (Figures 16 and 17), the transition region can be approximated as a straight line that passes through the origin. When the data begin to deviate from the straight line (at about  $j_2=20$  cm/sec), the flow is in the churn-turbulent regime.

c) churn-turbulent regime

As shown on Figures 4 and 5, the values of  $j_2$  for this regime range from 20 to 52 cm/sec as  $\alpha$  varies from 0.22 to 0.29. It is possible that it extends even farther than these values indicate, but it was impossible to explore the region beyond  $j_2$  equal to 52 cm/sec because of the limitations of the flowmeters.

This regime was characterized by non-uniform bubbles of non-uniform distribution. For the most part, the flow was dominated by large spherical cap bubbles which literally "shot" upward through the center of the flow in helical and zig-zag paths. This resulted in violent turbulent motion and turbulent convection currents which caused wide-spread bubble coalescence and shattering. The large bubbles entrained liquid in their wakes and carried it upward. This resulted in a net flow of liquid upward in a central core and downward in an annular region.

For  $L/D$  ratios of less than 5 for the 11.5 inch I.D. test section, the churn-turbulent regime was observed, but

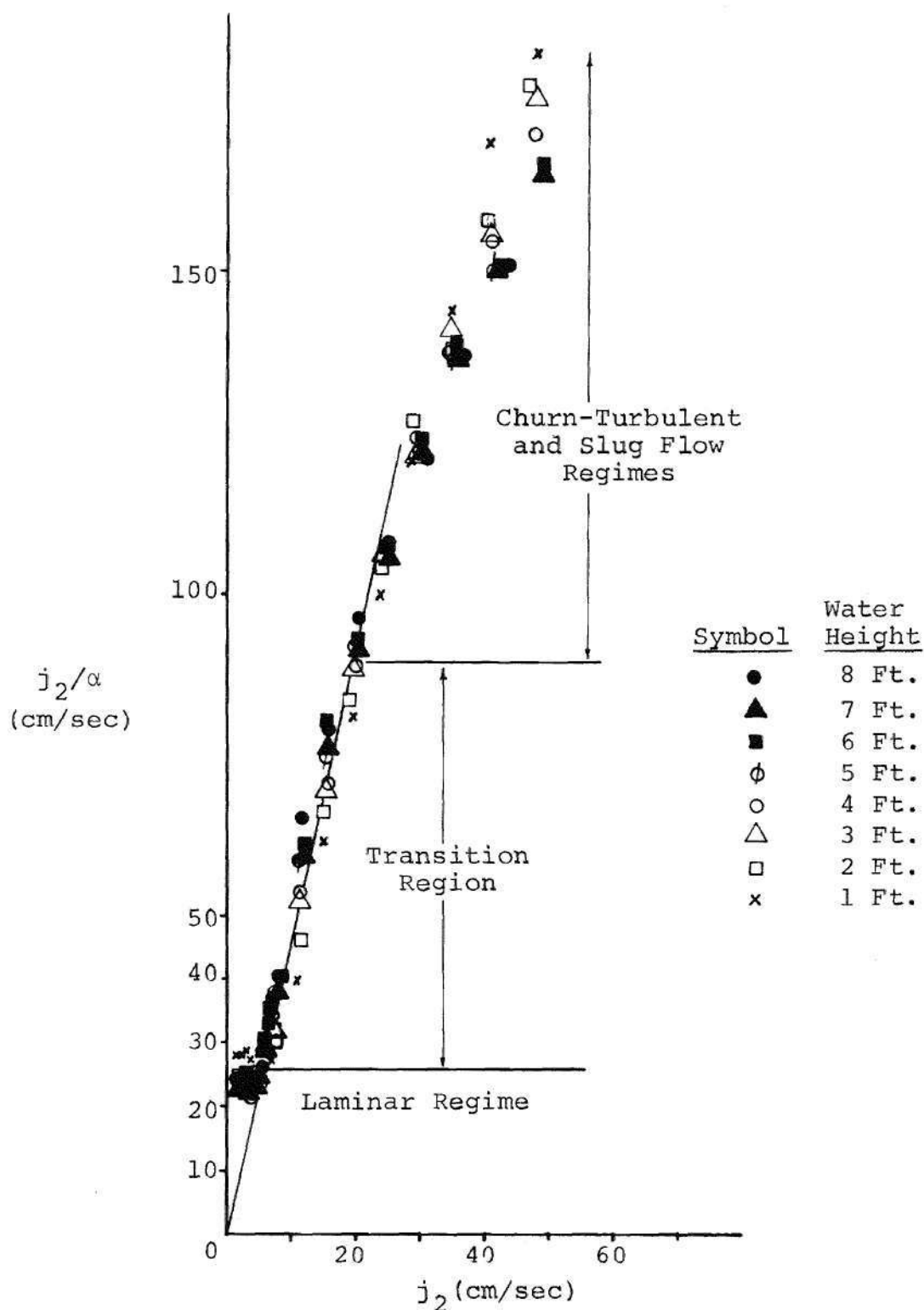


Figure 16. Velocity of the Gas Phase Versus Volumetric Flux Density for the 11.5 Inch I.D. Test Section Using the 70 $\mu$  Porous Plate

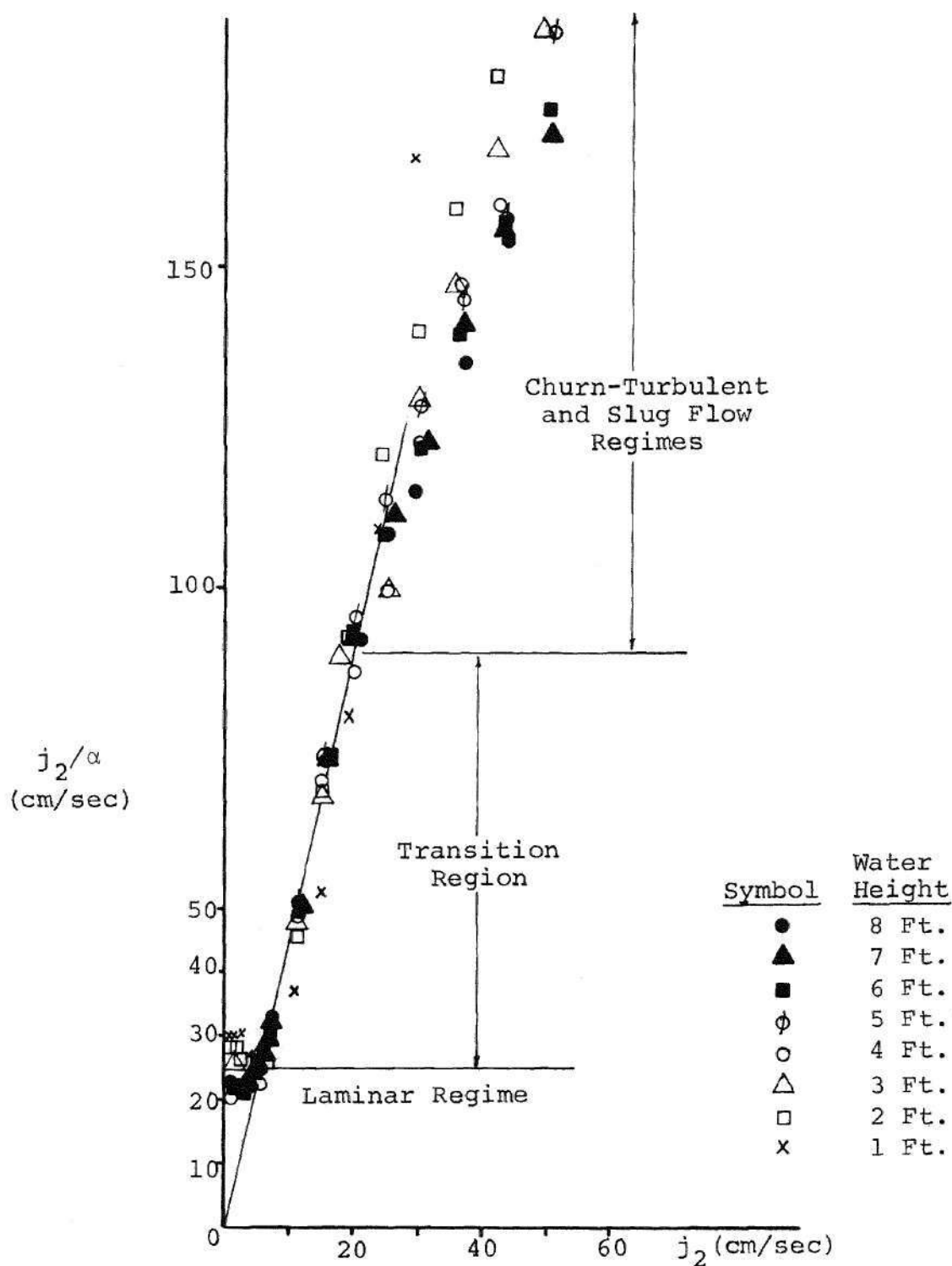


Figure 17. Velocity of the Gas Phase Versus Volumetric Flux Density for the 11.5 Inch I.D. Test Section Using the 120 $\mu$  Porous Plate

for  $L/D$  equal to 5 or more, the majority of the flow was in the slug flow regime. For the 4 inch I.D. pipe, the churn-turbulent regime was not present or at least was not observed.

From Figures 5 and 6, it can be seen that  $\alpha$  increases at a slow rate with increasing  $j_2$  as compared to the laminar region. It is also evident that for a fixed  $j_2$ ,  $\alpha$  is unaffected by plate porosity but increases with increasing  $L/D$ . The reason for this increase is that at greater water heights, the injected gas is under higher pressure and, thus, the density is greater. With more distance in which to rise and a greater initial density, the bubbles can expand to a larger size and, thus, the void fraction is larger.

On Figures 18 through 21, graphs are plotted of  $j_2/\alpha$  versus  $j_2$  for individual water heights. It is obvious that the churn-turbulent regime can be represented by a straight line as predicted by Zuber and Findlay [14]. Thus, if Equation (19) is used to analyze this regime,  $C_0$  should be the slope of the line, and the terminal velocity should be given by the intercept with the  $j_2/\alpha$  axis. As can be seen from the figures,  $C_0$  varies from 3.3 to 3.5 and  $u_t$  ranges from about 23 to approximately 28 cm/sec. The values of  $u_t$  are in line with the expected results, but the values of  $C_0$  are much higher than those suggested by Zuber and Findlay ( $C_0 = 1.0$  to  $1.5$ ). The reason for this is the profiles considered by Zuber and Findlay in their determination of  $C_0$  did not take into account the downward motion of the liquid

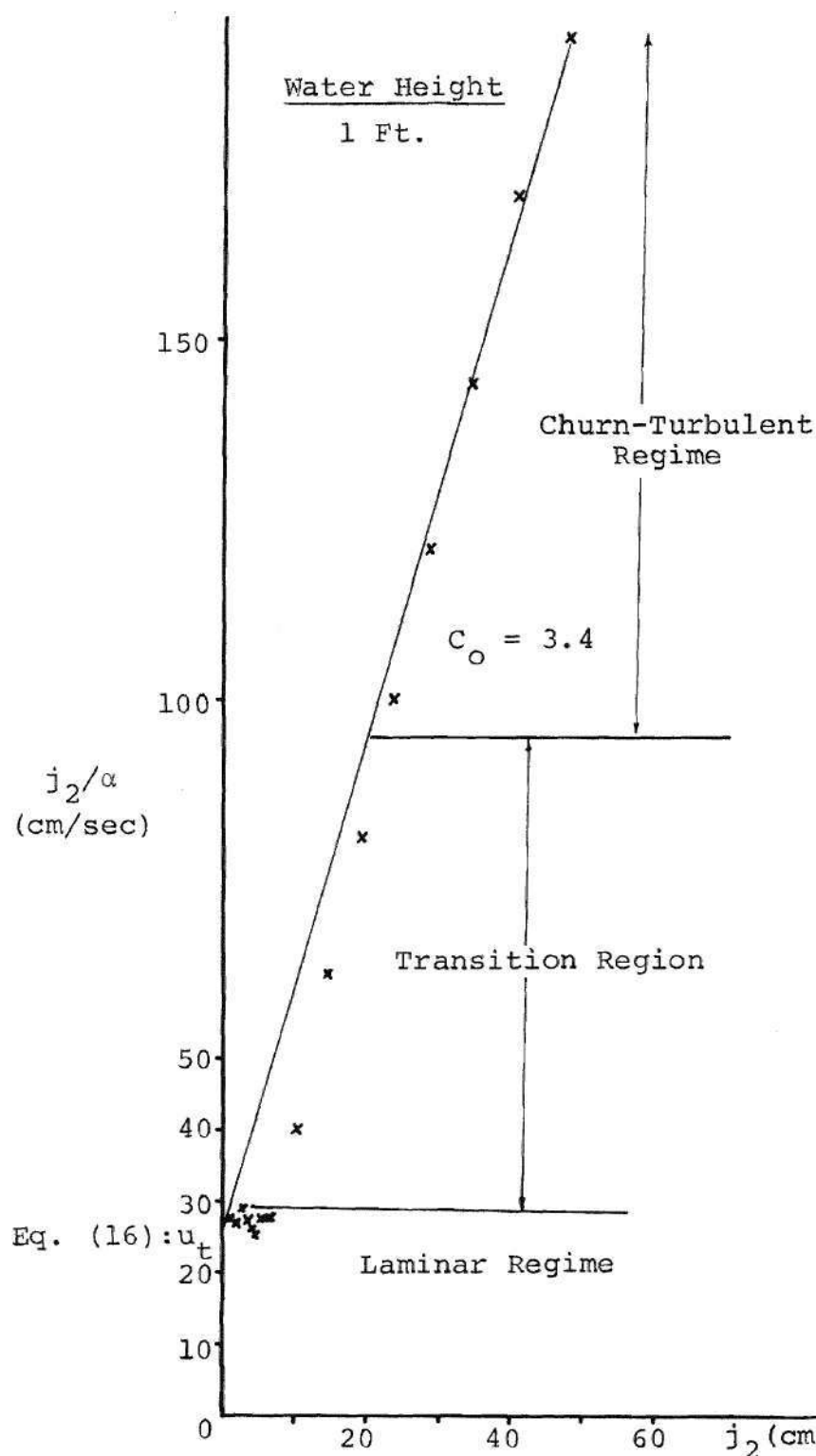


Figure 18. Velocity of the Gas Phase Versus Volumetric Flux Density for the 11.5 Inch I.D. Test Section Using the 70 $\mu$  Porous Plate

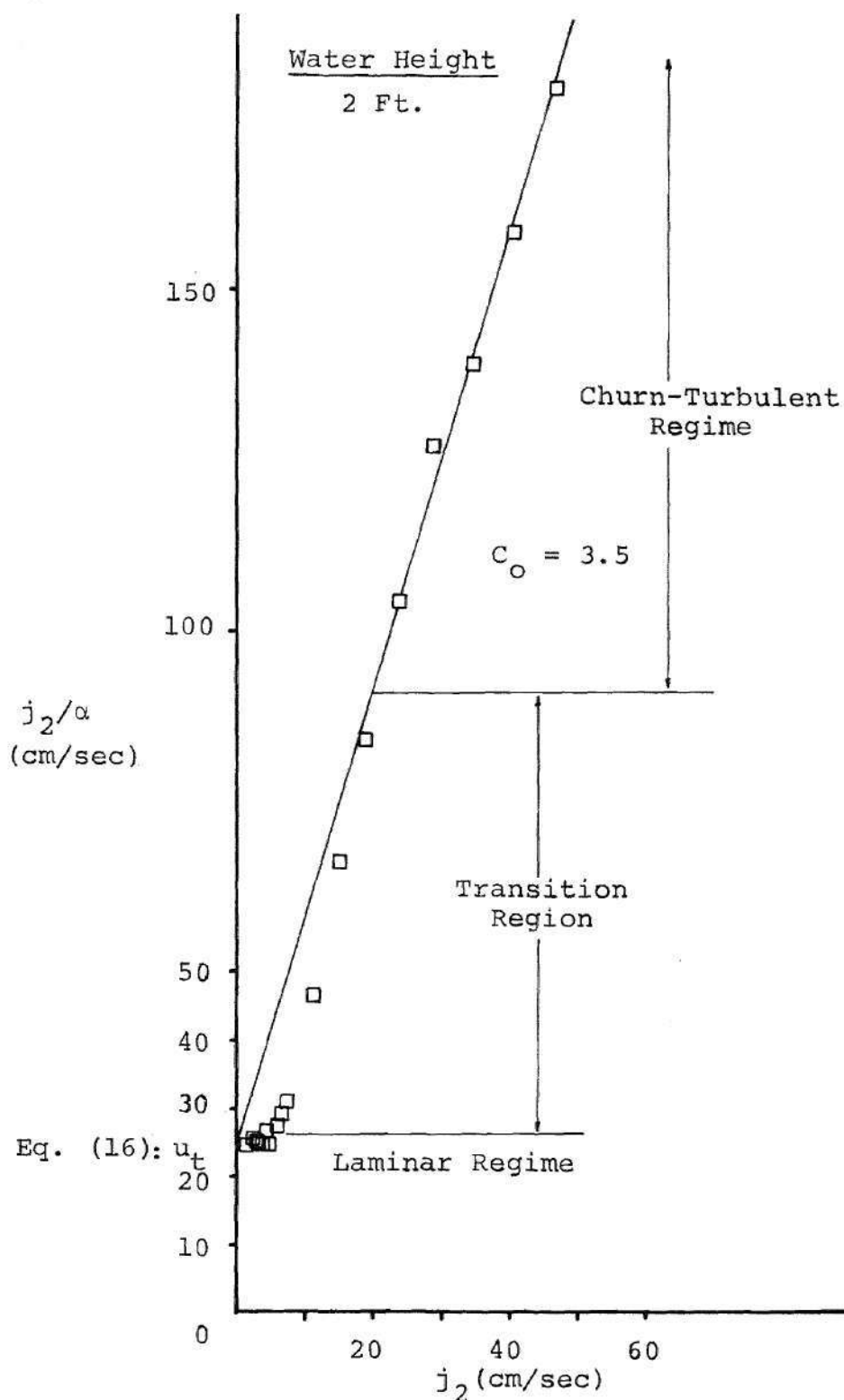


Figure 19. Velocity of the Gas Phase Versus Volumetric Flux Density for the 11.5 Inch I.D. Test Section Using the 70 $\mu$  Porous Plate



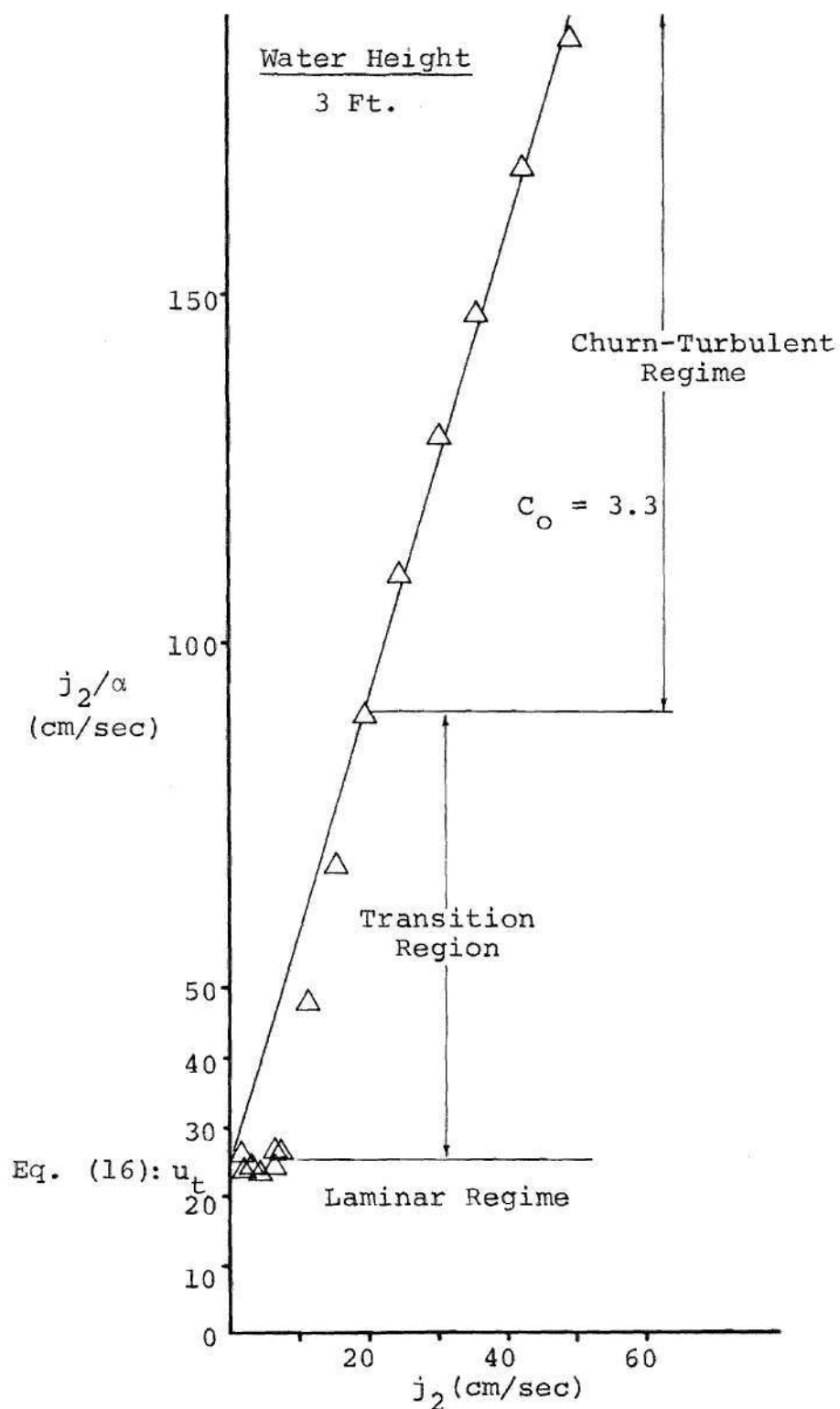


Figure 20. Velocity of Gas Phase Versus Volumetric Flux Density for the 11.5 I.D. Test Section Using the 120 $\mu$  Porous Plate

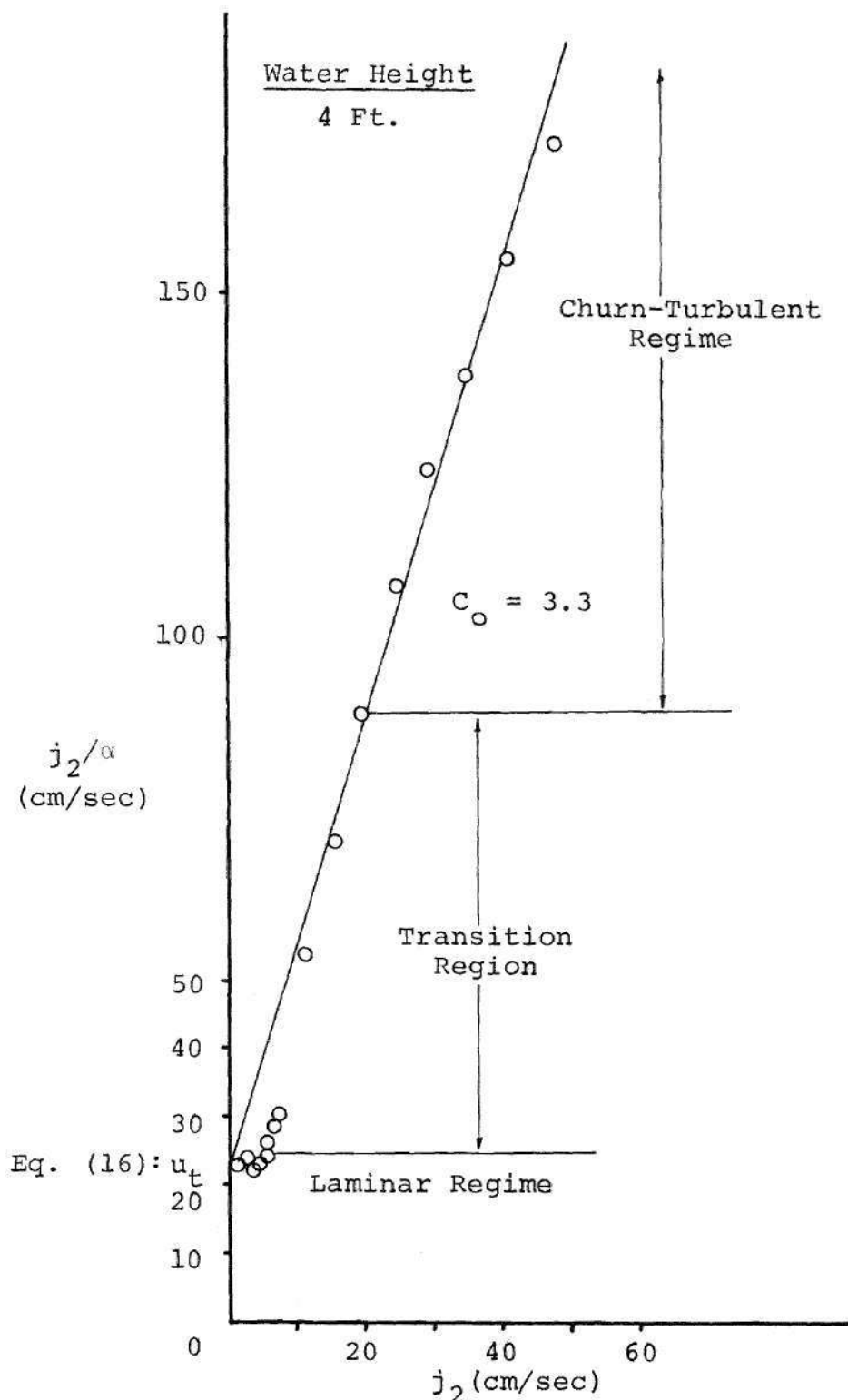


Figure 21. Velocity of the Gas Phase Versus Volumetric Flux Density for the 11.5 Inch I.D. Test Section Using the 70 $\mu$  Porous Plate

in the annulus of the flow. As mentioned in the Introduction, they considered profiles that ranged from flat to parabolic, whereas the profile needed to analyze the flow characteristic to this regime would have to have two minima, one maximum, and, therefore, two inflection points. However, there is another method for arriving at a value for  $C_o$ . This was suggested by Zuber [17] with the equation

$$C_o = (1+\phi) \frac{A}{A_c} \quad (24)$$

where  $\phi$  is the ratio of the volume of the liquid entrained by the bubble to the volume of the bubble,  $A$  is the total cross sectional area of the flow, and  $A_c$  is the cross sectional area of the core. If Equation (24) is used, the values of  $C_o$  as determined from Figures 18 through 21 are not out of line. (Consider, for example,  $\phi = 0.5$ , and  $A_c/A = 0.5$ , which are not bad estimates, then  $C_o = 3.0$ .)

d) slug flow regime

This regime was found to extend from  $j_2$  equal to 25 to about 50 cm/sec, and  $\alpha$  equal to 0.23 to approximately 0.33 (this value was determined from Figure 7). For the 11.5 inch I.D. test section, the slug flow regime appeared for values of  $L/D$  of about 5 or more. The reason it was not observed for  $L/D$  less than 5 was that for small  $L/D$  the flow did not have the time (i.e., the height) in which to develop

into slug flow. For the larger  $L/D$  ratios, there was enough water height so the slug flow regime could be attained.

The slug flow regime was characterized by large spherical cap bubbles with diameters approximately equal to the diameter of the test section. As in the churn-turbulent regime, the large bubbles entrained liquid in their wakes and transported it upward in a central core region while liquid flowed downward in the annulus.

Figures 5 and 6 show that the dependence of  $\alpha$  on  $L/D$  is the same as in the churn-turbulent regime (i.e.,  $\alpha$  increases with increasing  $L/D$  at fixed  $j_2$ ) and the effect of plate porosity is negligible. On Figures 22 through 25, graphs are plotted of  $j_2/\alpha$  versus  $j_2$  for the water heights of 5 to 8 feet. The straight line passing through  $u_t$  approximately equal to 25 cm/sec on the  $j_2/\alpha$  axis is the correlation as given by Equation (19) for the churn-turbulent regime. This line agrees with data for values of  $j_2$  between 20 and 25 cm/sec (which implies that some churn-turbulent regime is present in flows with  $L/D$  greater than 5), but does not agree with the data for  $j_2$  greater than 25 cm/sec. This is the slug flow regime, which can be represented as a straight line, as suggested by Zuber, Findlay [14], and others. (Equation (18) will be used in this analysis.) The slope of these lines for the slug flow regime as shown on Figures 22 through 25, gives values of  $C_0$  between 2.0 and 2.2, and the intercept with the  $j_2/\alpha$  axis is  $u_t$  equal to 59 cm/sec. This value for

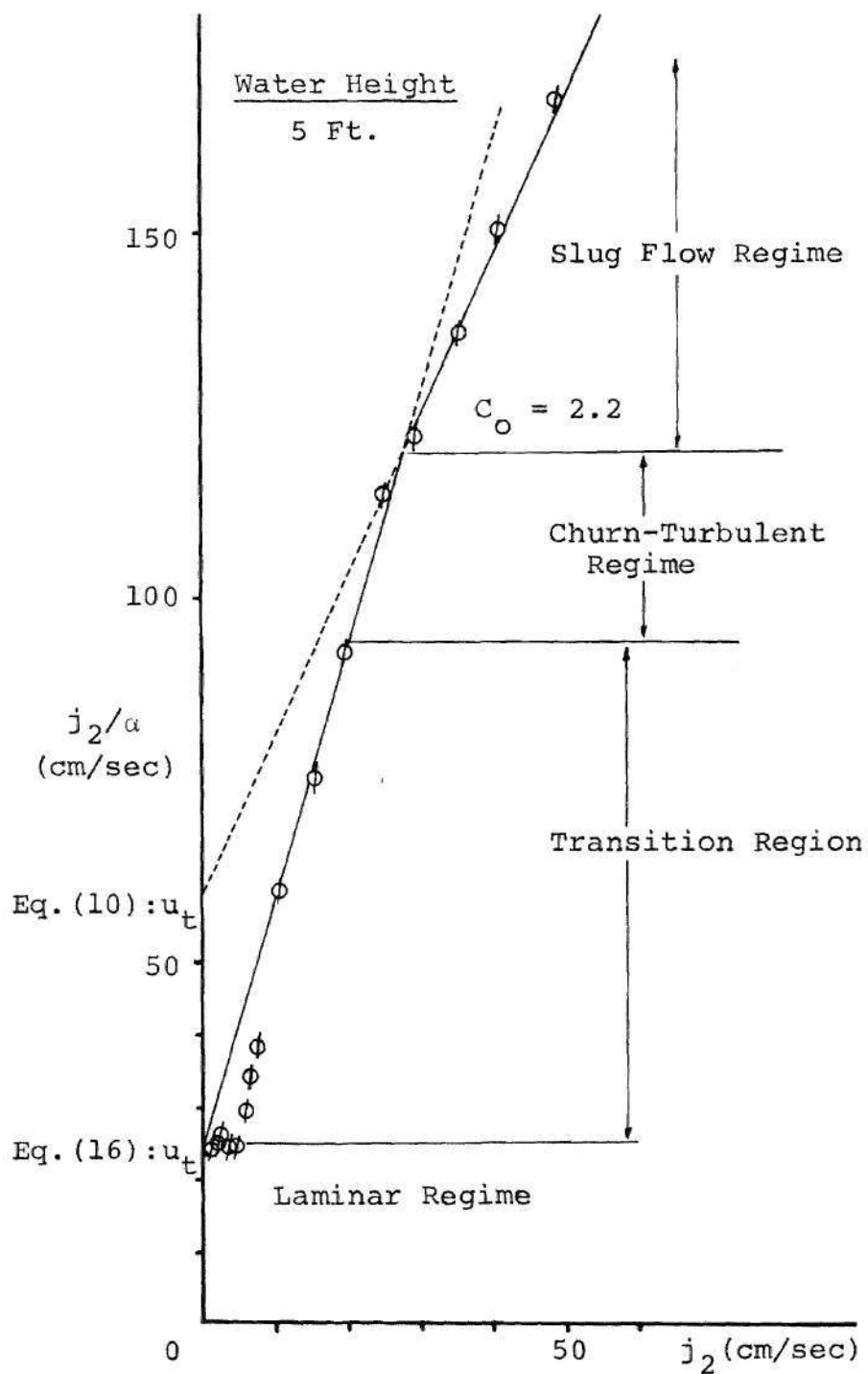


Figure 22. Velocity of the Gas Phase Versus Volumetric Flux Density for the 11.5 Inch I.D. Test Section Using the 70 $\mu$  Porous Plate

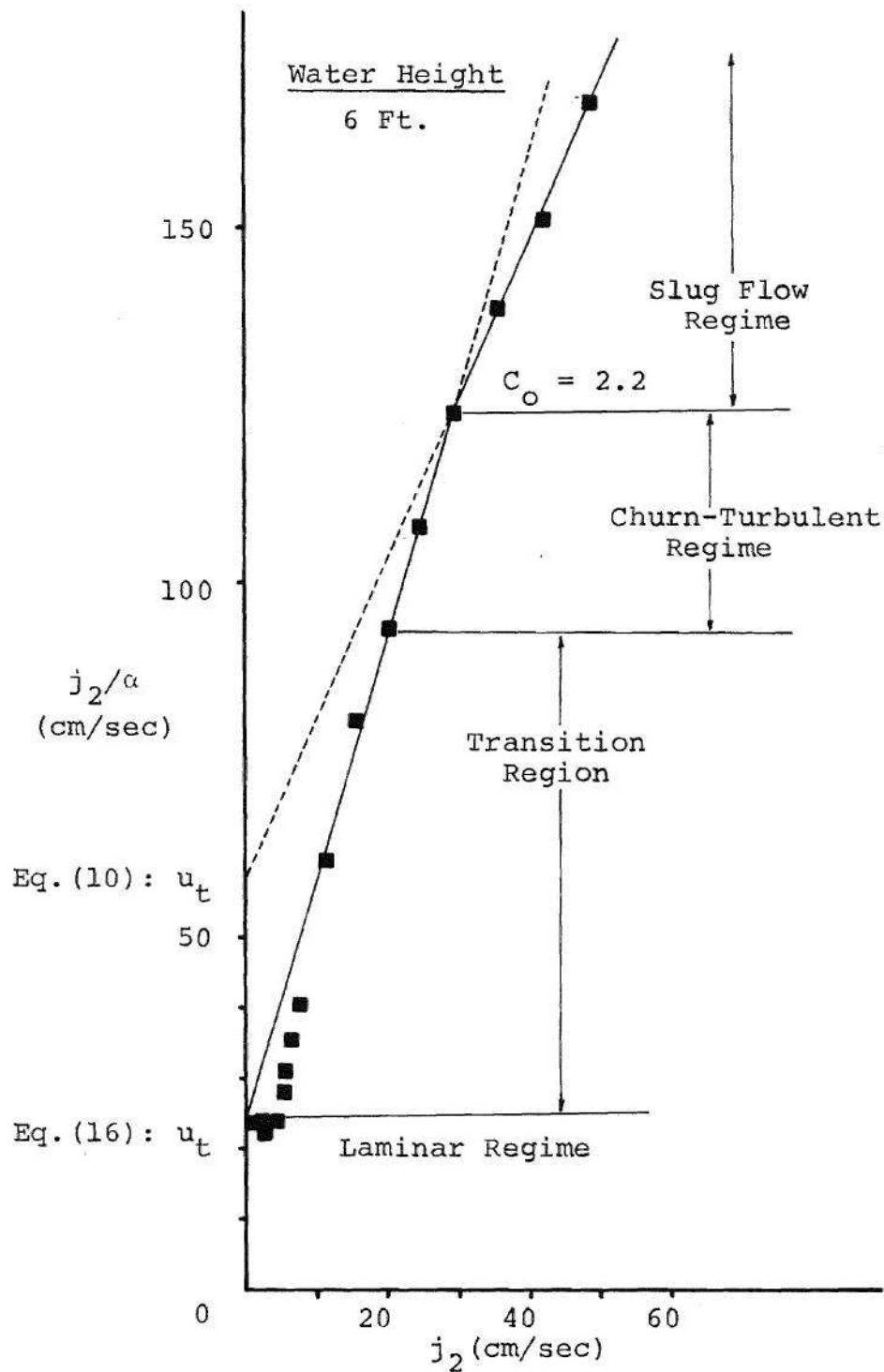


Figure 23. Velocity of the Gas Phase Versus Volumetric Flux Density for the 11.5 Inch I.D. Test Section Using the 70 $\mu$  Porous Plate

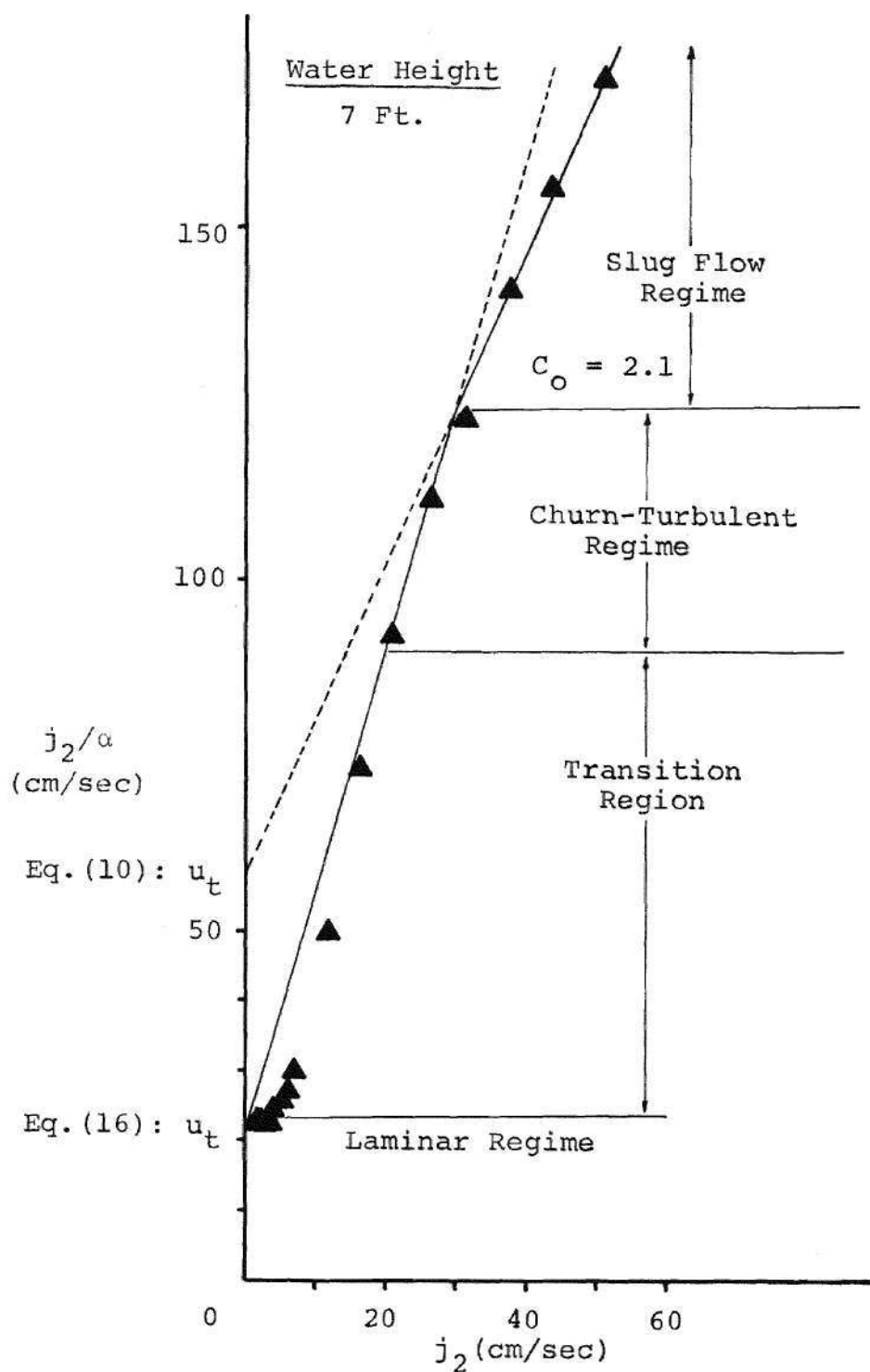


Figure 24. Velocity of Gas Phase Versus Volumetric Flux Density for the 11.5 Inch I.D. Test Section Using the 120 $\mu$  Porous Plate

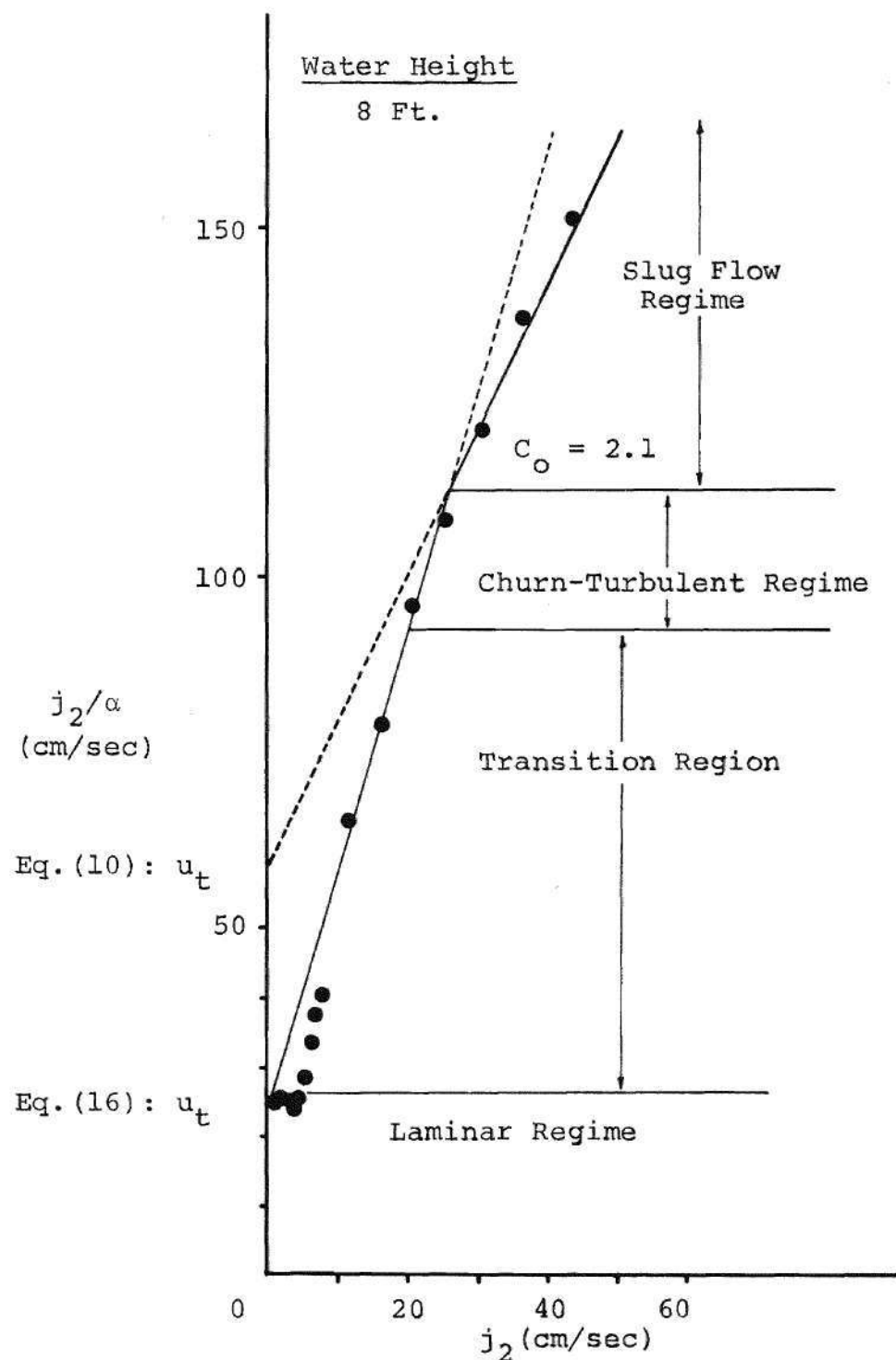


Figure 25. Velocity of the Gas Phase Versus Volumetric Flux Density for the 11.5 I.D. Test Section Using the 70 $\mu$  Porous Plate



the terminal velocity compares very well with the value of 59.1 cm/sec, which can be calculated using Equation (10) for a pipe with a diameter of 11.5 inches. The values of  $C_o$  are again high as compared to those obtained by Zuber and Findlay [14]. However, by using Equation (24) with the assumption that the area of the core to the total area is about 0.7 and with  $\phi$  equal to 0.5 (which gives  $C_o = 2.1$ ), the values of  $C_o$  as determined from the figures, are again reasonable.

On Figure 26, the data obtained for the 4 inch I.D. pipe plotted on a graph of  $j_2/\alpha$  versus  $j_2$  is presented. The slug flow regime can be represented by a straight line with a slope of about 2.4, and the intercept of this line with the  $j_2/\alpha$  axis gives a value of  $u_t$  equal to about 35 cm/sec. There is good agreement between this value of the terminal velocity and that as determined from Equation (10), which is 36.6 cm/sec for a pipe with a diameter of 4 inches.

As noted before, the churn-turbulent regime was difficult to detect in the 4 inch I.D. test section. The reason for this can be determined from Figure 26. The dotted line on this figure represents the correlation for the churn-turbulent regime. Both this line and the solid line, which represents the slug flow regime, are good fits to the data. Thus, graphically, the difference between these two regimes is almost imperceptible, and the churn-turbulent regime is difficult to detect. The churn-turbulent regime becomes

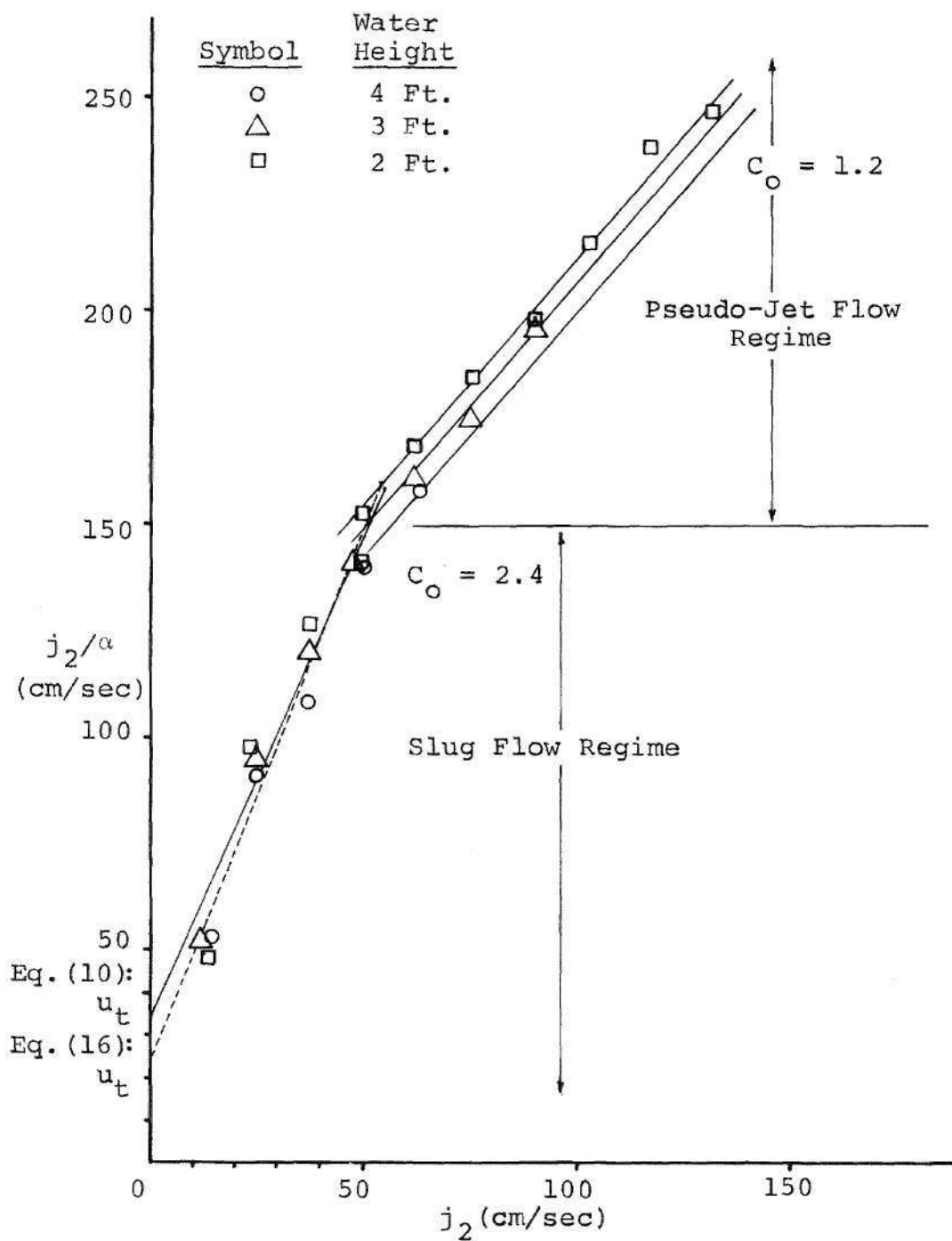


Figure 26. Velocity of the Gas Phase Versus Volumetric Flux Density for the 4.0 Inch I.D. Test Section Using the 70 $\mu$  Porous Plate

obvious only in larger diameter pipes.

e) pseudo-jet flow regime

This regime was experienced at volumetric flux densities of about 50 cm/sec and larger, (values that could not be attained in the 11.5 inch I.D. test section). The flow in this regime was characterized by a liquid annulus and a gas core much like a jet. The gas core was composed of a two-phase mixture of air and water droplets. The air rushing through the core of the tube attempted to hold the liquid at the wall. The liquid, however, would flow down at the wall, and at some point, the annulus would begin to thicken and restrict the flow. The annulus would then collapse, but almost immediately the liquid would be forced back to the wall. This process was repeated over and over.

As shown on Figure 26, the pseudo-jet flow regime can be approximated by straight lines as suggested by Zuber and Findlay [14]. The slope of these lines,  $C_0$ , is about 1.2, which agrees very well with the values noted by Zuber and Findlay ( $C_0 = 1.15$  to  $1.25$ ). As also noted by Zuber and Findlay, the intercepts of these lines with the  $j_2/\alpha$  axis yield values for the terminal velocity which are much higher than those for the churn-turbulent and slug flow regimes. Thus, the correlations used to describe the churn-turbulent and slug flow regimes cannot be used in this regime.

From Figure 7, it can be seen that  $\alpha$  increases with

increasing  $L/D$  for fixed  $j_2$ . On Figure 26, the effect of  $L/D$  is characterized by a shift of the lines of constant  $L/D$  parallel to each other. An analysis of this shifting phenomena was not possible, however, since insufficient information was available on the values of  $A_p$  (given by Equation (21)), which is dependent on the apparatus, and therefore the liquid height.

## CHAPTER IV

### CONCLUSIONS AND RECOMMENDATIONS

Four distinct two-phase flow regimes and a transition region have been experimentally obtained and analyzed for the process of bubbling air through water in a batch system. The characteristics and limits of each regime have been determined along with the effect of  $L/D$  on the flow system.

The laminar regime is characterized by uniformly sized and shaped bubbles of uniform distribution across the cross section. There is no bubble interactions in the form of bubble coalescence and shattering. The laminar regime occurs for void fractions up to 0.2 and volumetric flux densities up to 5 cm/sec. In this regime the void fraction increases very rapidly with increasing gas flow rate. The void fraction is independent of plate porosity and  $L/D$  but is linearly dependent on the gas flow rate (i.e., can be represented as a straight line passing through the origin with slope equal to the terminal rise velocity of a single bubble in an infinite medium). The terminal velocity is 24 cm/sec in this regime.

The transition region is characterized by non-uniform bubbles of non-uniform distribution. It occurs for volumetric flux densities between 5 and 20 cm/sec. The void fraction

fluctuates in value and is found to experience a net increase of 0.2. No conclusions can be made since a theory for this region is not currently available.

The churn-turbulent regime occurs for void fractions between 0.22 and 0.29 and volumetric flux densities of 20 to 52 cm/sec for  $L/D$  less than 5 and void fractions between 0.22 and 0.24 and flux densities between 20 and 25 cm/sec for  $L/D$  of 5 or greater. This regime is characterized by non-uniformly sized bubbles of non-uniform distribution. The cross section of the flow is divided into two regions: a central core in which large spherical cap bubbles entrain liquid and transport it upward, and an annular region which is caused by the return flow of liquid.

The slug flow regime occurs for values of volumetric flux density between 25 and 50 cm/sec and void fraction from 0.23 to 0.33 for  $L/D$  of 5 or greater. This regime is characterized by large spherical cap bubbles with diameters of approximately the same size as the test section. As in the churn-turbulent regime the cross section is divided into two regions.

The pseudo-jet flow regime occurs for volumetric flux densities of 50 cm/sec and greater and for void fractions between 0.35 and 0.60. This regime is characterized by a collapsing annular flow of a two-phase mixture of air and water droplets in the central core and an annular region of water.

The void fraction in the churn-turbulent, slug flow, and pseudo-jet regimes is independent of plate porosity but increases with increasing  $L/D$  for constant gas flow rates. The void fraction increases with increasing gas flow rate at a much slower rate in the churn-turbulent regime than in the laminar regime, at a slightly faster rate in the slug flow regime than in the churn-turbulent, and at a slightly faster rate in the pseudo-jet than in the slug flow regime.

The churn-turbulent, slug flow, and pseudo-jet flow regimes can be represented as straight lines on a plot of  $j_2/\alpha$  versus  $j_2$ . The slopes of these lines result in values of  $C_0$  equal to 3.3, 2.1, and 1.2, respectively. The terminal velocity for the size of bubbles in each regime (except for the pseudo-jet flow regime) is given by the intercept of these lines with the  $j_2/\alpha$  axis. The terminal velocity for the churn-turbulent regime is 25 cm/sec. For the 11.5 inch I.D. test section the terminal velocity in the slug flow regime is 59 cm/sec, and for the 4 inch I.D. test section it is 35 cm/sec. The effect of  $L/D$  on the pseudo-jet flow regime is to shift the lines of constant  $L/D$  parallel and downward for increasing  $L/D$ .

As a recommendation, it is suggested that these same experiments be undertaken for larger diameter test sections using perhaps different working fluids in order to obtain a more thorough understanding of the limits of the distinct regimes and of the effect of  $L/D$ . It is also recommended

that a theory be perfected for the prediction of  $C_o$  and that a complete analysis be performed on the pseudo-jet flow regime.



## APPENDIX A

## THE RISE OF SINGLE BUBBLES IN AN INFINITE MEDIUM

Figure 27 is a graph of the terminal velocity of rise of single bubbles in an infinite medium as a function of bubble size. It has been reproduced from the report of Haberman and Morton [4]. In the region AB the bubbles are small spheres for which Stokes' solution can be used. In BC the bubbles are again spheres but are not subject to Stokes' solution. In regions CD and DE the bubble shapes are spheroidal and spherical cap, respectively. The drag coefficients and terminal velocities for the various regions are given in Table 1 where

$$r_e = \left[ \frac{3}{4\pi} v_b \right]^{1/3}$$

and  $v_b$  is the bubble volume.

Peebles and Garber [5] also considered the terminal velocity of rise of a single bubble. Their results are shown in Table 2 where

$$Re_b = \frac{2\rho_l u_t R_b}{\mu_l}$$

$$G_1 = \frac{g\mu_1^4}{\rho_1\sigma^3}$$

$$G_2 = \frac{gR_b^4 u_t^4 \rho_1^3}{\sigma_3}$$

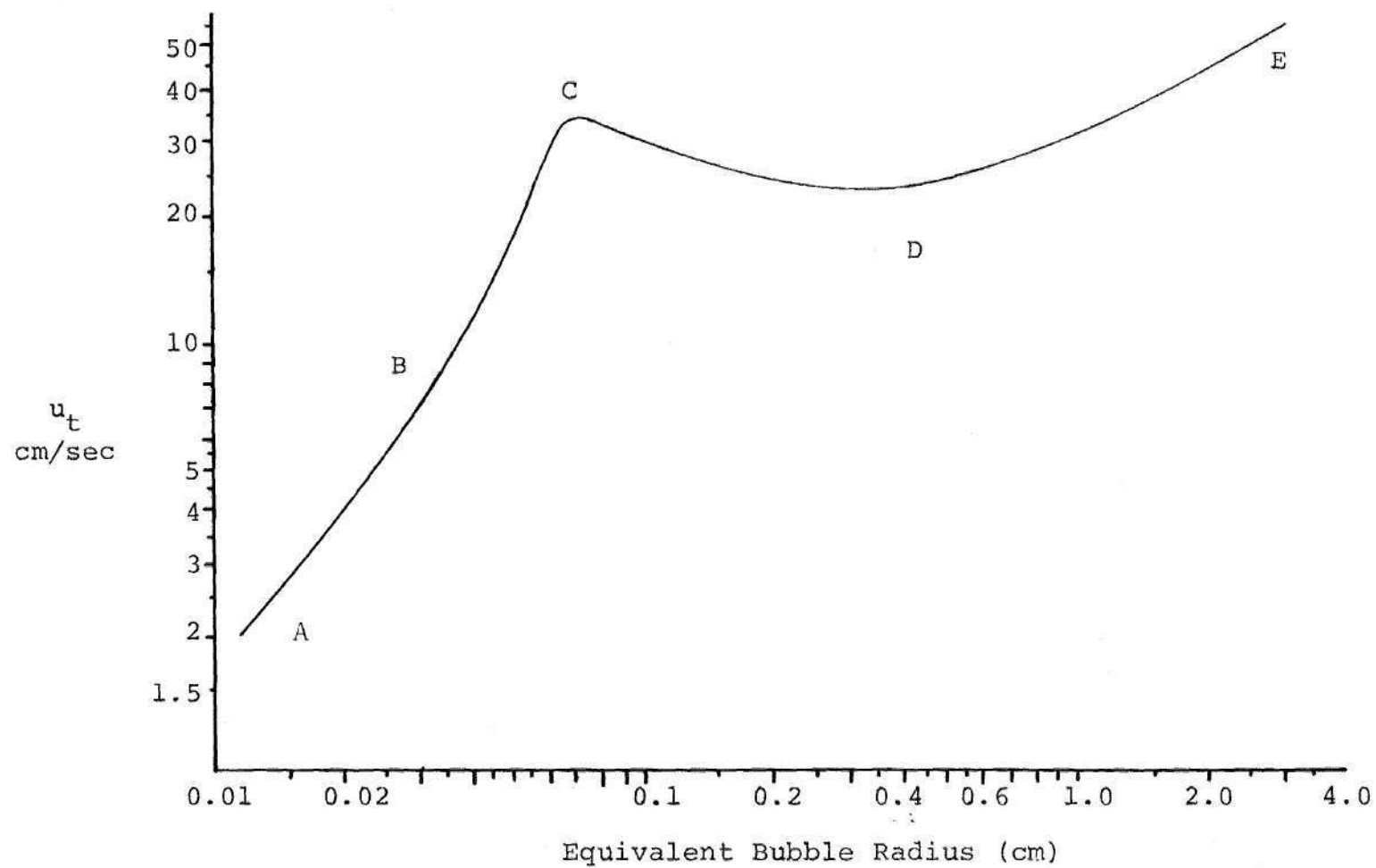


Figure 27. Terminal Velocity of Rise of Air Bubbles as a Function of Bubble Size

Table 1. Drag Coefficients and Terminal Velocities  
(for the regions given on Figure 27)

Region	$C_D$	$U_t$
AB	$24 \left( \frac{\mu_1}{\rho_1 u_t d} \right)$	$\frac{d^2 g (\rho_1 - \rho_2)}{18 \mu_1}$
BC	$18.3 \left( \frac{\mu_1}{\rho_1 u_t d} \right)^{0.68}$	$\left[ \frac{2}{27} \frac{g (\rho_1 - \rho_2)}{\rho_1} \left( \frac{\rho_1 d}{\mu_1} \right)^{2/3} \right]^{3/4}$
CD	$1.64 g \left( \frac{d}{2} \right)^4 \frac{u_t \rho_1}{\sigma^3}$	$1.35 \left[ \frac{\sigma}{\rho_1 d} \right]^{1/2}$
DE	2.6	$1.05 \left[ g \frac{\rho_1 - \rho_2}{\rho_1} r_e \right]^{1/2}$

Table 2. Terminal Velocity of Single Gas Bubbles in Liquids (according to Peebles and Garber [5])

Region	$U_t$	Range of Applicability
1	$\frac{2R_b^2(\rho_1 - \rho_2)g}{9\mu_1}$	$Re_b < 2$
2	$0.33g^{0.76} \left(\frac{\rho_1}{\mu_1}\right)^{0.52} R_b^{1.28}$	$2 < Re_b < 4.02G_1^{-2.124}$
3	$1.35 \left(\frac{\sigma}{\rho_1 R_b}\right)^{0.50}$	$4.02G_1^{-0.214} < Re_b < 3.10G_1^{-0.25}$ or $16.32G_1^{0.144} < G_2 < 5.75$
4	$1.18 \left(\frac{g\sigma}{\rho_1}\right)^{0.25}$	$3.10G_1^{-0.25} < Re_b$ $5.75 < G_2$

## APPENDIX B

## DETERMINATION OF VOLUMETRIC FLUX DENSITY

Since the flowmeters are calibrated for an exit pressure of 14.7 psia and an air temperature of 70°F, the meter readings have to be corrected for the varying pressures ( $P_o$ ) and temperatures ( $T_o$ ) that are obtained during experimentation. The corrected cfm value ( $Q_o$ ) is calculated by dividing the meter reading ( $Q$ ) by a correction factor given by

$$S = \sqrt{\frac{T_o}{530} \frac{14.7}{P_o}}^*$$

The volumetric flux density,  $j_2$ , is determined by considering the conservation of mass over the control volume shown on Figure 28. The mass flowing in is that passing through the exit of the flowmeter and is given  $\rho_o Q_o$ . The mass passes out of the control volume through the top of the porous plate. By assuming that air is a perfect gas and that bubbles are formed over the entire surface of the plate, the volumetric flux density in the tube is given as

---

\* This form of the correction factor is recommended by the manufacturer.

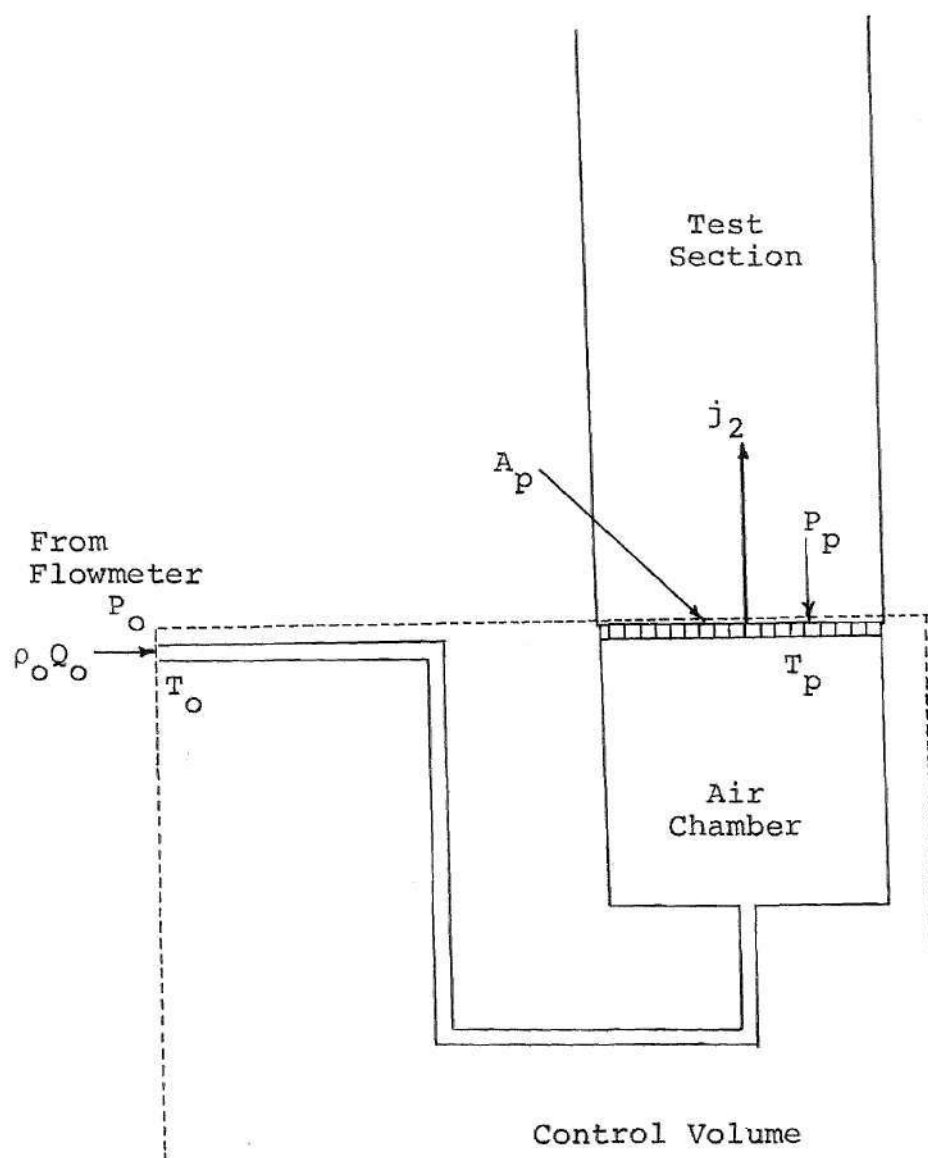


Figure 28. Control Volume for the Determination of the Volumetric Flux Density from Measurable Quantities

$$j_2 = \frac{Q}{A_{pl}} \left( \frac{P_o}{P_p} \right) \left( \frac{T_p}{T_o} \right) \frac{1}{S}$$

where  $A_{pl}$  is the cross sectional area of the porous plate,  $P_p$  is the pressure at the plate (which is equal to the atmospheric pressure plus the hydrostatic pressure of the water), and  $T_p$  is the temperature of the air passing through the porous plate.



## APPENDIX C

This appendix contains the data obtained during experimentation. The Flow Rate,  $Q$ , is the flowmeter reading. The pressure readings are given for the determination of the volumetric flux density,  $j_2$ , from the corrected flowmeter reading (as shown in Appendix B). The manometer readings are not given but, instead, they have been reduced to the values of void fraction as determined from Equation (22).

Table 3. Data for 11.5 Inch I.D. Test Section Using the 70 $\mu$  Porous Plate  
 $T_o = 75^\circ\text{F}$        $T_p = 70^\circ\text{F}$       Barometric Pressure = 14.45 psia

Q CFM	Water Height Ft.											
	1			2			3			4		
	$P_o$ psia	$j_2$ cm/sec	$\alpha$	$P_o$ psia	$j_2$ cm/sec	$\alpha$	$P_o$ psia	$j_2$ cm/sec	$\alpha$	$P_o$ psia	$j_2$ cm/sec	$\alpha$
1.8	14.45	1.20	.044	15.05	1.24	.050	15.70	1.29	.079	16.20	1.31	.056
3.0	14.45	2.00	.074	15.15	2.09	.082	15.80	2.17	.085	16.20	2.19	.089
4.0	14.45	2.67	.092	15.25	2.81	.112	15.85	2.90	.113	16.20	2.92	.121
5.0	14.45	3.34	.122	15.35	3.54	.144	15.85	3.63	.141	16.20	3.65	.163
6.0	14.45	4.01	.153	15.35	4.25	.161	15.90	4.37	.183	16.25	4.40	.186
7.0	14.45	4.68	.183	15.40	4.99	.204	15.90	5.10	.203	16.30	5.15	.210
8.0	14.50	5.35	.196	15.45	5.91	.215	15.90	5.83	.218	16.35	5.91	.221
9.0	14.55	6.05	.218	15.45	6.65	.226	15.95	6.60	.232	16.35	6.65	.231
10.0	14.65	6.81	.248	15.50	7.20	.236	15.95	7.32	.225	16.40	7.45	.244
15.0	14.85	10.45	.261	15.60	11.25	.243	16.00	11.00	.211	16.45	11.20	.207
20.0	15.45	14.75	.239	15.90	15.00	.226	16.25	15.10	.216	16.70	15.30	.216
25.0	15.80	19.10	.235	16.05	19.00	.226	16.50	19.30	.218	17.00	19.65	.221
30.0	16.10	23.60	.235	16.45	23.60	.226	16.90	24.00	.225	17.40	24.40	.226
35.0	16.50	28.40	.235	16.90	28.70	.226	17.35	29.10	.239	17.70	29.15	.234
40.0	17.05	34.30	.239	17.40	34.30	.247	17.85	34.75	.246	18.20	34.80	.252
45.0	17.65	40.55	.239	17.90	40.20	.254	18.35	40.75	.261	18.70	40.80	.263
50.0	18.40	48.00	.261	18.50	46.90	.262	18.95	47.40	.268	19.40	47.80	.279

Table 4. Data for 11.5 Inch I.D. Test Section Using the 70 $\mu$  Porous Plate  
 $T_o = 75^\circ\text{F}$        $T_p = 70^\circ\text{F}$       Barometric Pressure = 14.2 psia

Water Height Ft.												
5				6			7			8		
Q CFM	P <sub>o</sub> psia	j <sub>2</sub> cm/sec	$\alpha$	P <sub>o</sub> psia	j <sub>2</sub> cm/sec	$\alpha$	P <sub>o</sub> psia	j <sub>2</sub> cm/sec	$\alpha$	P <sub>o</sub> psia	j <sub>2</sub> cm/sec	$\alpha$
1.8	16.60	1.33	.055	16.80	1.33	.055	17.20	1.34	.060	17.70	1.37	.054
3.0	16.65	2.22	.089	16.85	2.23	.091	17.20	2.24	.095	17.70	2.28	.080
4.0	16.65	2.96	.122	16.85	2.98	.130	17.20	3.00	.129	17.70	3.05	.122
5.0	16.70	3.72	.153	16.90	3.73	.160	17.25	3.76	.165	17.70	3.81	.158
6.0	16.70	4.46	.185	16.90	4.48	.186	17.25	4.51	.189	17.75	4.60	.181
7.0	16.75	5.22	.190	16.95	5.24	.186	17.30	5.30	.198	17.75	5.36	.189
8.0	16.80	6.00	.203	16.95	5.99	.193	17.35	6.06	.207	17.75	6.13	.183
9.0	16.85	6.78	.198	17.00	6.79	.189	17.40	6.85	.203	17.80	6.91	.186
10.0	16.85	7.54	.198	17.10	7.60	.186	17.45	7.65	.201	17.85	7.75	.192
15.0	16.90	11.35	.190	17.20	11.50	.189	17.60	11.60	.195	18.10	11.85	.181
20.0	17.15	15.45	.206	17.30	15.50	.193	17.75	15.65	.204	18.25	16.00	.202
25.0	17.45	19.85	.215	17.70	20.00	.214	18.10	20.20	.220	18.55	20.50	.213
30.0	17.80	24.55	.214	18.00	24.60	.228	18.45	25.00	.236	18.95	25.35	.234
35.0	18.15	29.40	.240	18.50	29.95	.242	18.80	30.00	.246	19.45	30.80	.255
40.0	18.65	35.10	.257	18.95	35.40	.256	19.25	35.50	.261	20.00	36.70	.268
45.0	19.20	41.20	.274	19.55	41.80	.277	19.75	41.40	.276	20.60	43.20	.286
50.0	19.85	48.20	.287	20.20	48.70	.291	20.50	48.75	.294	---	---	--

Table 5. Data for 11.5 Inch I.D. Test Section Using the 120 $\mu$  Porous Plate  
 $T_o = 75^\circ\text{F}$        $T_p = 70^\circ\text{F}$       Barometric Pressure = 14.3 psia

Water Height Ft.												
1				2			3			4		
Q CFM	P <sub>o</sub> psia	j <sub>2</sub> cm/sec	$\alpha$	P <sub>o</sub> psia	j <sub>2</sub> cm/sec	$\alpha$	P <sub>o</sub> psia	j <sub>2</sub> cm/sec	$\alpha$	P <sub>o</sub> psia	j <sub>2</sub> cm/sec	$\alpha$
1.8	14.30	1.20	.040	15.25	1.29	.047	15.75	1.30	.051	16.15	1.32	.058
3.0	14.30	2.00	.067	15.30	2.15	.075	15.75	2.18	.092	16.20	2.21	.094
4.0	14.40	2.69	.089	15.30	2.87	.107	15.80	3.01	.125	16.25	2.96	.132
5.0	14.45	3.38	.128	15.35	3.61	.140	15.80	3.76	.163	16.25	3.70	.164
6.0	14.50	4.08	.155	15.40	4.35	.172	15.80	4.51	.191	16.30	4.46	.201
7.0	14.60	4.80	.178	15.45	5.10	.204	15.85	5.14	.216	16.30	5.20	.227
8.0	14.70	5.55	.200	15.50	5.86	.230	15.85	5.86	.241	16.30	5.95	.243
9.0	14.80	6.28	.245	15.55	6.61	.258	15.95	6.65	.248	16.35	6.72	.250
10.0	15.10	7.21	.276	15.65	7.44	.262	16.00	7.41	.278	16.40	7.50	.264
15.0	15.30	11.00	.293	15.75	11.25	.247	16.10	11.25	.234	16.55	11.40	.234
20.0	15.65	15.20	.289	15.95	15.30	.221	16.40	15.40	.227	16.80	15.55	.222
25.0	15.95	19.55	.245	16.35	19.80	.215	16.75	19.85	.222	17.30	20.30	.233
30.0	16.30	24.25	.222	16.75	24.70	.204	17.20	24.80	.227	17.70	25.20	.230
35.0	16.80	29.70	.178	17.25	30.10	.215	17.75	30.30	.234	18.10	30.40	.248
40.0	17.35	35.50	.178	17.80	36.00	.226	18.20	36.00	.245	18.70	36.50	.248
45.0	17.95	42.10	.200	18.35	42.35	.236	18.85	42.70	.254	19.25	43.00	.270
50.0	18.75	49.90	.222	19.10	50.00	.247	19.50	49.90	.268	19.90	50.20	.286

Table 6. Data for 11.5 Inch I.D. Test Section Using the 120 $\mu$  Porous Plate  
 $T_o = 75^\circ\text{F}$        $T_p = 70^\circ\text{F}$       Barometric Pressure = 14.3 psia

Water Height Ft.												
5				6			7			8		
Q CFM	P <sub>o</sub> psia	j <sub>2</sub> cm/sec	$\alpha$	P <sub>o</sub> psia	j <sub>2</sub> cm/sec	$\alpha$	P <sub>o</sub> psia	j <sub>2</sub> cm/sec	$\alpha$	P <sub>o</sub> psia	j <sub>2</sub> cm/sec	$\alpha$
1.8	16.55	1.33	.063	17.05	1.36	.058	17.40	1.37	.060	17.85	1.39	.058
3.0	16.65	2.24	.099	17.05	2.26	.102	17.45	2.29	.099	17.90	2.32	.097
4.0	16.70	3.00	.135	17.10	3.02	.137	17.50	3.07	.134	17.90	3.09	.131
5.0	16.70	3.76	.173	17.15	3.79	.176	17.55	3.85	.172	17.95	3.88	.168
6.0	16.75	4.52	.203	17.20	4.58	.200	17.60	4.65	.189	18.00	4.67	.200
7.0	16.75	5.27	.232	17.25	5.36	.207	17.65	5.44	.211	18.00	5.45	.213
8.0	16.80	6.05	.236	17.25	6.13	.228	17.70	6.24	.229	18.05	6.25	.221
9.0	16.85	6.86	.244	17.30	6.93	.236	17.75	7.05	.235	18.10	7.06	.231
10.0	16.85	7.62	.249	17.30	7.70	.242	17.75	7.83	.241	18.20	7.91	.239
15.0	17.05	11.65	.232	17.50	11.75	.232	17.90	11.90	.238	18.35	12.00	.237
20.0	17.35	15.90	.214	17.75	15.95	.218	18.25	16.35	.223	18.60	16.35	.221
25.0	17.70	20.50	.215	18.05	20.50	.221	18.50	20.80	.226	19.00	21.10	.230
30.0	18.10	25.40	.224	18.45	25.45	.235	18.95	26.60	.238	19.35	26.00	.239
35.0	18.60	30.80	.240	18.95	30.90	.253	19.35	31.20	.253	19.80	29.80	.260
40.0	19.25	37.20	.257	19.50	36.25	.263	19.95	37.30	.265	20.35	37.30	.276
45.0	19.90	44.00	.270	20.05	43.20	.276	20.45	43.60	.280	20.95	44.00	.286
50.0	20.70	51.80	.278	20.80	50.60	.291	21.15	51.00	.298	---	---	--

Table 7. Data for 4.0 Inch I.D. Test Section Using the 70 $\mu$  Porous Plate  
 $T_o = 75^\circ\text{F}$        $T_p = 70^\circ\text{F}$       Barometric Pressure = 14.4 psia

Q CFM	Water Height Ft.								
	2			3			4		
	$P_o$ psia	$j_2$ cm/sec	$\alpha$	$P_o$ psia	$j_2$ cm/sec	$\alpha$	$P_o$ psia	$j_2$ cm/sec	$\alpha$
2.0	15.40	11.85	.245	15.85	11.05	.232	16.25	12.10	.230
4.0	15.45	23.80	.243	15.90	24.15	.254	16.40	24.55	.270
6.0	15.60	36.30	.285	15.95	36.40	.303	16.45	37.00	.312
8.0	15.70	48.80	.319	16.00	48.80	.345	16.55	49.80	.356
10.0	15.80	61.50	.366	16.20	62.00	.386	16.65	62.80	.396
12.0	15.90	74.60	.404	16.35	75.50	.430			
14.0	16.10	88.50	.447	16.60	90.25	.458			
16.0	16.25	102.50	.475						
18.0	16.40	117.00	.490						
20.0	16.50	131.50	.531						
25.0	17.10	173.50	.583						

## REFERENCES

1. Siemes, W., "Gasblasen in Flussigkeiten," *Chemical Ingenieur Technik*, Volume 26, page 614, 1954.
2. Wallis, G. B., "Some Hydrodynamic Aspects of Two-Phase Flow and Boiling," *Proceedings of the International Heat Transfer Conference*, page 319, 1961.
3. Wallis, G. B., *One Dimensional Two-Phase Flow*, McGraw-Hill, New York, 1969.
4. Thornton, J. D., "Spray Liquid-Liquid Extraction Columns," *Chemical Engineering Science*, Volume 5, page 201, 1956.
5. Peebles, F. N. and Garber, H. J., "Studies on the Motion of Gas Bubbles in Liquid," *Chemical Engineering Progress*, Volume 49, Number 2, page 88, 1953.
6. Harmathy, T. Z., "Velocity of Large Drops and Bubbles in Media of Infinite and Restricted Extent," *AIChE Journal*, Volume 6, page 281, 1960.
7. Levich, V. G., *Physicochemical Hydrodynamics*, Prentice-Hall, Inc., Englewood Cliffs, New Jersey, 1962.
8. Zuber, N. and Hench, J., "Steady State and Transient Void Fraction of Bubbling Systems and Their Operating Limits, Part I: Steady State Operation," General Electric Report Number 62GL100, July, 1962.
9. Haberman, W. L. and Morton, R. D., "An Experimental Investigation of the Drag and Shape of Air Bubbles Rising in Various Liquids," Navy Department, David Taylor Model Basin, Report 802, September, 1953.
10. Nicklin, D. J., "Two-Phase Bubble Flow," *Chemical Engineering Science*, Volume 17, page 673, 1962.
11. Nicklin, D. J., Wilkes, J. O., and Davidson, J. F., "Two-Phase Flow in Vertical Tubes," *Transactions of the Institute of Chemical Engineers*, Volume 40, page 61, 1962.
12. Griffith, P. and Wallis, G. B., "Two-Phase Slug Flow," *ASME Transactions, Journal of Heat Transfer*, Volume 83, Section C, page 307, 1961.

13. White, E. T. and Beardmore, R. H., "The Velocity of Rise of Single Cylindrical Air Bubbles Through Liquids Contained in Vertical Tubes," *Chemical Engineering Science*, Volume 17, page 351, 1962.
14. Zuber, N. and Findlay, J. A., "The Effects of Non-Uniform Flow and Concentration Distributions and the Effect of the Local Relative Velocity on the Average Volumetric Concentration in Two-Phase Flow," General Electric Report Number GEAP-4592, April, 1964.
15. Brodkey, R. S., *The Phenomena of Fluid Motions*, Addison-Wesley Publishing Company, Massachusetts, 1967.
16. Govier, G. W. and Aziz, D., *The Flow of Complex Mixtures in Pipes*, Van Nostrand Reinhold Company, New York, 1972.
17. Zuber, N., Private Communication.